PHILOSOPHICAL TRANSACTIONS OF THE ROYAL SOCIETY A MATHEMATICAL, PHYSICAL & ENGINEERING SCIENCES

The Profiles of Axially Symmetric Menisci

J. F. Padday

Phil. Trans. R. Soc. Lond. A 1971 **269**, 265-293
doi: 10.1098/rsta.1971.0031

THE PROFILES OF AXIALLY SYMMETRIC MENISCI

By J. F. PADDAY
Research Laboratories, Kodak Limited, Wealdstone, Harrow, Middlesex

(*Communicated by D. Tabor, F.R.S.—Received 2 June* 1970)

CONTENTS

The shape and forces of axisymmetric menisci have been calculated for sessile drops, pendant drops and liquid bridge profiles. The tables of Bashforth & Adams have been extended into the liquid bridge region by generating profiles beyond the 180° angle of their study, and into regions covered by a much wider range of shape factor.

Numerical integration of the Laplace equation was performed by using a first-order method originally proposed by Lord Kelvin but adapted and modified for use with high-speed computers.

Tables have also been generated, by the same techniques, of profiles of a wide range of asixymmetric menisci that do not cross the axis of symmetry. Such tables include the shape of a meniscus formed by a rod at a free liquid surface. This second group of tables greatly extended the region over which liquid bridge shapes could be obtained.

Closed menisci of the type of Bashforth & Adams's tables are defined by one shape factor β, but open menisci require two parameters to identify their shape. The general properties of these shape factors are discussed.

The volume of any part of the meniscus bounded by two horizontal planes has also been derived and its relationship to the forces acting between the planes is given.

The tables (400 pages)† are not reproduced here but the main features of these profile shapes are summarized and discussed with the aid of graphs.

† It is planned to publish the full set of tables or otherwise to make them available by photographic duplication.

Vol. 269. A. 1197. (Price 15*s*. (£0.75) U.S. $1.95) 23 [Published 5 February 1971

1. Introduction

The pressure difference, Δp, across an interface separating two immiscible fluid phases is given by the well-known Laplace equation (Laplace 1805)

$$\Delta p = \gamma(1/R_v + 1/R_h), \tag{1}$$

where γ is the interfacial tension and R_v and R_h are the principal radii of curvature in the vertical and horizontal planes respectively. Plateau (1873) showed that the mass of material forming the membrane of a soap film was so small that the sum of the curvatures possessed some constant

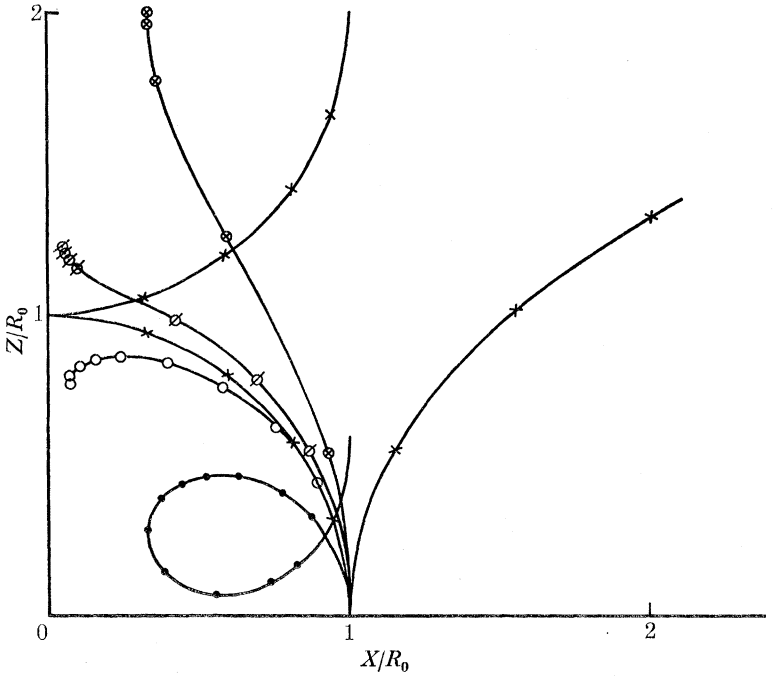

Figure 1. Profiles of axisymmetric soap films.

	R_v/R_h (max)	R_v/R_h (min)	shape
•	0.5	−0.5	nodoid
○	0.9	−0.9	nodoid
×	1.0	—	circle
×	—	−1.0	catenoid
⌀	1.1	−1.1	unduloid
⊗	2.0	−2.0	unduloid

value independent of vertical height. The shapes of these soap films are extensively reviewed by Bakker (1928) and have been used by other workers to give approximate shapes of profiles of liquid interfaces even when gravitational forces cannot be neglected (Melrose 1966). Profiles of Plateau's soap films may be obtained by integrating equation (1) by using elliptic integrals of the first and second kind (Princen 1969).

Equation (1) may be expressed in dimensionless form as

$$\left(\frac{R_0}{R_v} + \frac{R_0}{R_h}\right) = \frac{\Delta p R_0}{\gamma}, \tag{2}$$

where the constant multiplier, R_0, may be any constant linear dimension. In figure 1, solutions of this equation obtained by integration are plotted with R_0 taken as the maximum value of R_h(max)

or the minimum value $R_h(\min)$. Thus at the starting-point the curve shape is characterized completely by the ratio $R_v(\max)/R_h(\max)$ or by $R_v(\min)/R_h(\min)$. In figure 1 X and Z are the horizontal and vertical coordinates respectively, reduced to dimensionless values by dividing by the common multiplier of equation (2). The shape of all soap film profiles that cross the axis of symmetry must be circular and all profiles that do not cross the axis of symmetry must be bounded by two surfaces each of which cut the axis of symmetry and the soap film. The shape of soap films supported between two planes depends on the pressure difference Δp, the surface tension force (equal to 2γ because there are two liquid vapour surfaces in a soap film) and the scale $R_h(\max)$ which in turn determines the ratio $R_v/R_h(\max)$ and which determines the type of profile: nodoid, unduloid or catenoid.

The pressure, Δp, across the surface of a meniscus separating two immiscible fluids of unequal density varies with the vertical height Z to give

$$\left(\frac{1}{R_v}+\frac{1}{R_h}\right)=\frac{\rho g}{\gamma}(Z+Z_0), \tag{3}$$

where ρ is the relative density between the two phases, g is the gravitational acceleration and Z_0 the hydrostatic height of some fixed point on the meniscus from the free flat surface of the liquid/vapour interface. In dimensionless form equation (3) becomes

$$\left(\frac{R_0}{R_v}+\frac{R_0}{R_h}\right)=\frac{\rho g R_0^2}{\gamma}\left(\frac{Z}{R_0}+\frac{Z_0}{R_0}\right), \tag{4}$$

where

$$\frac{\rho g R_0^2}{\gamma}\frac{Z_0}{R_0}=2. \tag{5}$$

Bashforth & Adams (1883) made $R_0 = b$, the radius of curvature at an origin where the profile crossed the axis of symmetry, so that $R_v = R_h = b$ at this origin. By expressing the hydrostatic height in a similar dimensionless form they produced the well-known equation

$$\frac{b}{R_v}+\frac{b}{R_h}=\frac{\beta Z}{b}+2, \tag{6}$$

where

$$\beta=\rho g b^2/\gamma. \tag{7}$$

Equations (3), (4) and (6) are essentially the same second-order differential equations which, as is well known, may not be solved in closed form (Buff 1960).

Early attempts to solve equation (3) are reviewed in Bakker (1928). Among these Verschaffelt (1918) produced several solutions of the equation for profiles which under certain conditions allowed some terms to be simplified or dropped out altogether. Lord Kelvin (1886) produced a number of profiles of sessile drops and pendant drops using a geometrical construction method. This method has been used more recently (Cross & Picknett 1963) and is essentially a first-order graphical integration method applied to a second-order equation. Bashforth & Adams (1883) integrated equation (6), using hand-calculated coefficients of Taylor series and obtained tables of X/b and Z/b for values of β from 0.1 to 100 for sessile drops, and from -0.1 to -4.0 for some pendant drop profiles. In the pendant-drop calculations they assigned negative values to β. Bashforth & Adams's tables have been extended slightly by Blaisdell (1940) and Staicopolus (1962, 1963, 1967) for sessile-drop conditions and by others (Andreas, Hauser & Tucker 1938; Fordham 1948; Niederhauser & Bartell 1950; Mills 1953; Stauffer 1965) for pendant-drop conditions. All these tables are collected together in one volume (Padday 1969).

All published tables of meniscus profiles are limited to $\phi = 0$–$180°$ for sessile-drop conditions, and to less than one cycle for pendant-drop conditions: ϕ is the angle between R_h and the axis of symmetry as shown in figure 2. Thus no tables exist for liquid bridges formed by axially symmetric menisci of liquid held between two parallel horizontal planes by two regular solid surfaces. Also the range of the shape factor β covered by existing tables does not extend to large enough values to be useful with problems involving large diameters. Furthermore, the shapes of menisci that do not cross the axis of symmetry, such as describe the profiles obtained with the Du Nouy ring or with a vertical rod at a free liquid surface do not appear to have been published, in comprehensive tabular form, though they have been investigated by Huh & Scriven (1968).

In recent years many attempts have been made to compute the profiles of menisci not covered by existing tables, by restricting conditions so that the mathematics may be simplified. Macfarlane & Tabor (1950) and Pietsch & Rumpf (1967) have assumed that the profile of a liquid bridge between a sphere and a plate and between two spheres are approximately circular when the amount of liquid forming the bridge is small. Ku, Ramsey & Clinton (1968) omit R_h altogether to obtain a closed form solution of equation (3) and Derjaguin (1946) uses boundary conditions to obtain a solution. Nodoid approximations of Plateau have been used (Radushkevich 1952; Clark, Haynes & Mason 1968; Fisher 1926), but in exact form for the case of two liquids of equal density by Mason & Clark (1965). Nutt (1960) obtains solutions of the rod-in-free-surface meniscus by using boundary conditions where one of the principal radii of curvature was omitted from the solution.

Profiles obtained with a rod-in-a-free-surface of liquid (exact within the limits of computation error) are given in the form of graphs by White & Tallmadge (1965) and both as graphs and tables by Huh & Scriven (1969), but neither set of results is suitable for liquid bridge profiles between two solid surfaces. The only published profiles of successive cycles of a gravity distorted nodoid showing the shape of liquid bridges appears to be those of Lord Kelvin produced by a graphical construction method. These, unfortunately, are too few in number and too inaccurate to be of use.

In this study tables of nodoids and unduloids distorted by gravity have been computed to cover the cases of sessile drops, pendant drops and their associated liquid bridges and also the liquid bridge conditions derived from meniscus profiles that do not cross the axis of symmetry and the associated rod-in-free-surface profiles.

2. The generation of axisymmetric surface profiles and their volumes

Integration method

Equation (3) may be written in differential form as

$$\pm \frac{\mathrm{d}^2z/\mathrm{d}x^2}{\{1+(\mathrm{d}z/\mathrm{d}x)^2\}^{\frac{3}{2}}} \pm \frac{\mathrm{d}z/\mathrm{d}x}{x\{1+(\mathrm{d}z/\mathrm{d}x)^2\}^{\frac{1}{2}}} = \frac{\rho g}{\gamma}(Z+Z_0). \tag{8}$$

As integration of equation (4) or (8) cannot be performed analytically the problem becomes one of predicting values of the term $\mathrm{d}^2z/\mathrm{d}x^2$ in equation (8), or its related variable R_v, so that a step-by-step integration process may be attempted. In this treatment the values $\mathrm{d}x$ and $\mathrm{d}z$ were derived on the basis that R_v did not change significantly when small enough steps were taken so that the real change in R_v could be derived directly from either equation without a knowledge of $\mathrm{d}^2z/\mathrm{d}x^2$.

The quantities ϕ, Z, X, R_v and R_h and their dimensionless counterparts form the variable terms which govern the shape of a profile, and the method by which they are defined is given in figure 2. In this figure the definitions are assigned according to the type of profile: sessile drop, pendant drop and liquid bridge. Starting with some self-consistent and easily identified values of ϕ, X, Z, R_v and R_h, the rest of the profile was generated with the aid of high-speed computers to perform the step-by-step numerical integration procedure outlined above.

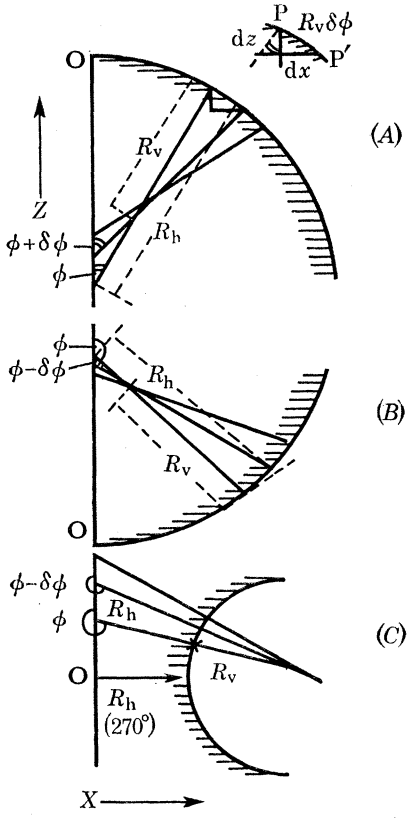

FIGURE 2. Construction method for axially symmetric menisci. (A) Sessile drop, free liquid surface is above O. (B) Pendant drop, free liquid surface is above 0. (C) Liquid bridge, free liquid surface is usually below O.

The procedure adopted here is best described mathematically by the following steps:

(i) Designate a self-consistent set of starting values of the terms R_0, R_v/R_0, R_h/R_0, $\rho g R_0^2/\gamma$, Z/R_0, Z_0/R_0, ϕ and X/R_0 according to equation (4) and also consistent with

$$R_h/R_0 = \frac{X/R_0}{\sin\phi}, \quad \text{when} \quad X/R_0 > 0. \tag{9}$$

(ii) Assign a small value to the increment $\delta\phi$ and calculate increment $\delta X/R_0$ using

$$\delta X/R_0 = (R_v/R_0)\,\delta(\sin\phi); \tag{10}$$

then add $\delta X/R_0$ to X/R_0.

(iii) Calculate $\delta Z/R_0$ according to

$$\delta Z/R_0 = (-R_v/R_0)\,\delta(\cos\phi); \tag{11}$$

then add $\delta Z/R_0$ to Z/R_0.

(iv) With the new values of $(X+\delta X)/R_0$ and $\phi+\delta\phi$ a new value R_h/R_0 is calculated from equation (9).

(v) With the new values of R_h/R_0 and $(Z+\delta Z)/R_0$ a new value of R_v/R_0 is calculated according to equation (4), using the predetermined value of $\rho g R_0^2/\gamma$. For the condition $R_0 = b$ equations (6) and (7) are more suitable to calculate the new value of R_v/R_0 but for other conditions equation (4) is used, with R_0 defined as $R_h(270°)$ and the associated shape factor β' given by

$$\beta' = \rho g R_h(270°)^2/\gamma. \tag{12}$$

(vi) The new value of R_v/R_0 at $(\phi+\delta\phi)$ is compared with the old value R_v/R_0 at (ϕ) for a change in sign. Such change indicates an inflexion point such as is found with pendant drops and when it occurs further calculations must be continued by changing the sign of $\delta\phi$ so that at the next step the gradient of the profile reaches a maximum or minimum value.

TABLE 1. STARTING VALUES FOR PROFILE SHAPE CALCULATIONS

parameter	closed meniscus tables (Bashforth & Adams's tables)		open meniscus tables	
	sessile drop, distorted nodoid	pendant drop, distorted unduloid	distorted nodoid	distorted unduloid
ϕ	0°	180°	270°	90°
$\delta\phi$	+0.02°	−0.02°	±0.02°	±0.02°
base measurement R_0	b	b	$R_h(270°)$	$R_h(270°)$
X/R_0	1.0	1.0	1.0	1.0
Z/R_0	0	0	0	0
Z_0/R_0	$2/\beta$	$2/\beta$	$1/\beta\left(\frac{R_0}{R_v}+\frac{R_0}{R_h}\right)$	
R_v/R_0	1.0	1.0	to be assigned	
R_h/R_0	1.0	1.0	<-1	>-1
			-1.0	-1.0
shape factor to be assigned	$\beta = \frac{\rho g b^2}{\gamma}$		$\beta' = \frac{\rho g R_h(270°)^2}{\gamma}$	

The procedure above enables successive values of X/R_0, Z/R_0, R_v/R_0 and R_h/R_0 to be derived for any integer multiple of $\delta\phi$. Two sets of tables have been compiled by this method. The first set follows the method of Bashforth & Adams whereby the base measurement, R_0, is designated as b, the radius of curvature at the point where the meniscus crosses the line of symmetry. The second set represents the profiles of menisci that do not cross the axis of symmetry and have generally been classed as liquid bridge menisci. The starting conditions for both sets of tables are given in table 1.

The computations were carried out on an I.B.M. 1130 computer using extended precision with printout at each increment of 5° from 0° to 360° for the sessile drop shapes. To obtain the pendant-drop profiles, a starting value of $\phi = 180°$ was used instead of 0° and the increment $\delta\phi$ made negative. This was regarded as more realistic than using Bashforth & Adams's device of assigning a negative value of β for these profiles. Thus pendant-drop profiles would start with a negative value of $\delta\phi$ so that the angle would successively reduce until the first inflexion point is reached. Here $\delta\phi$ changes sign and ϕ now increases to the second inflexion point where $\delta\phi$ changes sign again. Most pendant-drop tables were compiled for angles of ϕ from 180° to the second inflexion point, while a few were generated over many cycles in order to obtain successive bridge or neck conditions for a given shape factor.

The range of the shape factor β, of the tables of this study, extends from 10^{-6} to 10^{6} with

increments of β varying according to the position in the range. The increments were relatively small in the range $\beta = 0.1$ to 10^3 and very large outside this range. The range of β for pendant-drop profiles covered the range 10^{-4} to 10^2, though it should be noted that very little useful information was obtained for values greater than $\beta = 8$. The pendant-drop values of β in these tables correspond to the negative values given in Bashforth & Adams's tables.

In order to obtain profiles of menisci which do not cross the axis of symmetry one must clearly find some different but well-defined starting-point. The starting-point chosen for the liquid-bridge tables of this study was at the midpoint of the neck of the liquid-bridge profile of figure 2 C, i.e. where $\phi = 270°$. The starting values of the profile parameters for these conditions are given in table 1. The base measurement R_0 is taken as the value of $R_h(270°)$ because the radius b no longer has any significance. The profiles were generated in both directions, i.e. $\pm \delta\phi$ over a range usually extending 90° in either direction or to the first inflexion point, whichever appeared sooner. Both the value of β', the shape constant, and the value of $R_v/R_h(270°)$ determine the actual shape of the profile. Therefore for each selected value of β' separate tables were generated for each of a series of starting values of $R_v/R_h(270°)$. Some tables were generated over many cycles to investigate changes of shape of successive bridge conditions with a constant value of β'.

Shape factors

In making equation (3) dimensionless the physical constants are grouped together as already shown in equation (5). R_0, the common multiplier, may be any well-defined linear dimension of the profile. Bashforth & Adams used the radius of curvature, b, at the axis of symmetry for R_0. Many other dimensions such as the maximum radius of a sessile or pendant drop, the vertical radius of curvature, $R_v(90°)$, at the maximum diameter, the vertical height from free surface, Z_0, or the vertical radius of curvature at the minimum value of X, i.e. $R_v(270°)$, of a liquid-bridge profile may be used as a base measurement.

In this study the shape factors used are Bashforth & Adams's β (equation (7)) to the base b, the liquid bridge shape factor β' (equation (12)) to the base $R_h(270°)$ and the liquid-bridge shape factor β'' to the base $R_v(270°)$ (for figures 14 to 16) where

$$\beta'' = \rho g R_v(270°)^2/\gamma. \tag{13}$$

In table 2 these shape factors are defined and their related values derived from the computed tables for sessile-drop conditions. They were obtained from the value of $R_h/b(270°)$ and $R_v/b(270°)$ by multiplying β by the second power of $R_h/b(270°)/b$ or $R_v(270°)/b$ to give β' and β'' respectively. The physical significance of these characteristic dimensions is shown in figure 3 where the shaded side of the profile indicates that phase of greater density. This figure is similar to that produced by Lord Kelvin (1886) but with the differences that here the relation between distorted nodoids (sessile drop) and distorted unduloids (pendant drops) is given unambiguously and that the shapes are somewhat more accurately derived.

The radius of curvature b of the sessile-drop tables is virtually impossible to measure experimentally, therefore almost any other base value is more convenient. Sugden (1921) converted Bashforth & Adams's tables to a base $R_h(90°)$, i.e. the maximum radius of a sessile drop, whilst Smolders (1961) and later Tawde & Parvatikar (1951, 1954, 1958) did the same thing, the former to obtain the surface tension from a sessile-drop profile, the latter to obtain corrections for the rise of liquid in a capillary tube.

In addition to the profile shape it will be seen (from table 3) that the force acting in the meniscus

and the volume enclosed between two parallel horizontal planes and the meniscus profile have also been calculated in the tables. These calculations were carried out in the following way.

Forces acting on a meniscus and meniscus volume

It is implicit in earlier studies that axisymmetric profiles crossing the axis of symmetry possess certain simple volume/force relations: for instance the total force supporting a pendant drop

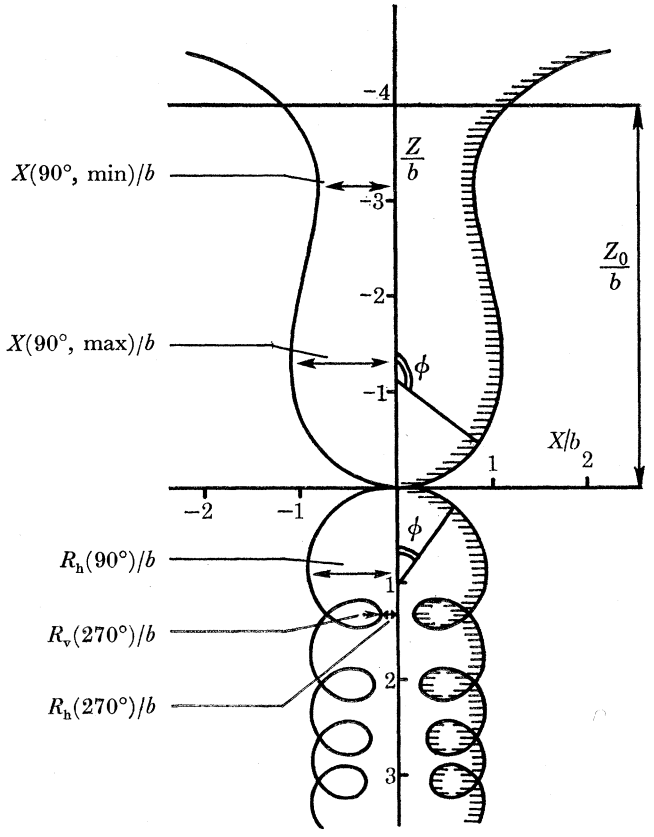

FIGURE 3. Characteristic dimensions of sessile and pendant drop profiles for $\beta = 0.5$, $b = 1.0$.

TABLE 2. SHAPE FACTORS

Bashforth & Adams	base $R_h(270°) = 1.0$		base $R_v(270°) = 1.0$	
β	β' (equation (12))	$\frac{R_v(270°)}{R_h(270°)}$	β'' (equation (13))	$\frac{R_h(270°)}{R_v(270°)}$
0	0	−1.0	0	−1.0
0.01	0.000000 (4)	−0.986963	0.000000 (4)	−1.013209
0.1	0.000327	−0.889628	0.000258	−1.124065
1.0	0.063589	−0.561770	0.020068	−1.780088
5.0	0.588890	−0.363725	0.077480	−2.756907
10.0	1.141913	−0.306775	0.109856	−3.259719
50.0	3.472324	−0.221882	0.170949	−4.506892
100	4.948845	−0.197727	0.193794	−5.057471
500	9.518964	−0.157801	0.237032	−6.337115
1000	11.954798	−0.145238	0.252174	−6.885264
10000	22.034576	−0.115102	0.291924	−8.687951
100000	35.171252	−0.095446	0.320410	−10.477095
1000000	51.609856	−0.081431	0.342225	−12.280342

PHILOSOPHICAL TRANSACTIONS OF THE ROYAL SOCIETY A MATHEMATICAL, PHYSICAL & ENGINEERING SCIENCES

equals the mass of the drop times the gravitational acceleration. For a sessile drop a similar equilibrium of forces has been demonstrated (Padday 1963).

It is well known (Gillespie & Rose 1968; Cross & Picknett 1968; Princen 1968; Derjaguin 1968) that the total force due to surface effects contains two terms, one due to capillary pressure acting across the whole horizontal surface and another due to the surface tension pull adding a further extra force at the triple phase boundary.

If the total force acting on a horizontal plane crossing an axisymmetric meniscus is F, then

$$\begin{aligned} F &= \pi X^2 (Z + Z_0)\, \rho g - 2\pi X \gamma \sin\phi \\ &= \pi X^2 \left(\frac{1}{R_v} + \frac{1}{R_h}\right) \gamma - 2\pi X \gamma \sin\phi, \end{aligned} \tag{14}$$

which rearranged in dimensionless form, gives

$$\frac{F}{\rho g R_0^3} = \pi \frac{\gamma}{\rho g R_0^2} \frac{X^2}{R_0^2} \left(\frac{R_0}{R_v} + \frac{R_0}{R_h}\right) - \frac{2\pi\gamma}{\rho g R_0^2} \frac{X}{R_0} \sin\phi, \tag{15}$$

where R_0 is again some linear dimension of the meniscus profile.

The force columns of tables 3 A and B were derived using equation (15) with b as the appropriate base value R_0. The force column of table 3 C, however, required the use of equation (16) which is merely equation (15) with the sign of the second term changed,

$$\frac{F}{\rho g R_h(270°)^3} = \frac{\pi}{\beta'} \left[\frac{X}{R_h(270°)}\right]^2 \left[\frac{R_h(270°)}{R_v} + \frac{R_h(270°)}{R_h}\right] + \frac{2\pi}{\beta'} \frac{X}{R_h(270°)} \sin\phi. \tag{16}$$

This change of sign was important because in compiling the liquid bridge data (table 3 C) the sessile-drop profile of figure 3 was first turned upside down (rotated through 180°) to give the captive-bubble profile. It was then necessary to change the sign of the X/R_0 coordinate arbitrarily so as to conform to the usual sign convention of an X coordinate. Although this gave general consistency to the signs it was sometimes easier to adopt some arbitrary system and designate signs by inspection.

The force as here derived is directly related to the volume of liquid forming the meniscus. Bashforth & Adams (1883) and Bouasse (1924) recognized these relations, the latter author giving an extensive phenomenological description of volume relations, the former authors a calculation of some of their values.

It has been shown (Padday 1963) that the forces acting on a closed meniscus (i.e. cutting the axis of symmetry) may be derived by using Archimedes's principle as shown in figure 4. For the sessile drop, A, or the pendant drop, B, the first term of equation (15) represents the reduced force acting on the cylindrical volume LL′A′A obtained by rotating either figure on its vertical axis of symmetry. The second term represents the surface tension force corresponding to that force on the volume LL′A′OA. This second force is positive for the sessile-drop meniscus and negative for the pendant-drop profile. Thus the difference between capillary pressure and surface tension forces gives the shaded volumes in figures 4 A and 4 B—the volumes of the respective drops.

It should be noted that the total force acting on the sessile drop, A, at the plane EE′ is less than that at CC′ because the volume of the sessile drop at EE′ is decreased by the volume of the vapour bridge which has not been formed at CC′.

The force acting on the vapour bridge at EE′ of figure 4 A is equivalent to the volume of EPE′D′C′B′A′OABCD which equals the volume of the cylinder E′EMM′ because at EE′ the only vertical force acting is capillary pressure. The force acting on the vapour bridge at DD′ is

PHILOSOPHICAL TRANSACTIONS OF THE ROYAL SOCIETY A MATHEMATICAL, PHYSICAL & ENGINEERING SCIENCES

greater than at EE′ and corresponds to the force on the volume of the cylinder EE′M′M plus the volume of the bridge E′PEDD′ which again equals the force on the volume of liquid forming the sessile drop DD′C′B′A′OABC.

In figure 4*C* the force acting on a liquid bridge is that of an apparently unbounded meniscus. Therefore the force on the volume of liquid in the shaded area of the liquid bridge is derived according to equation (16). It is this force that is included in table 3c.

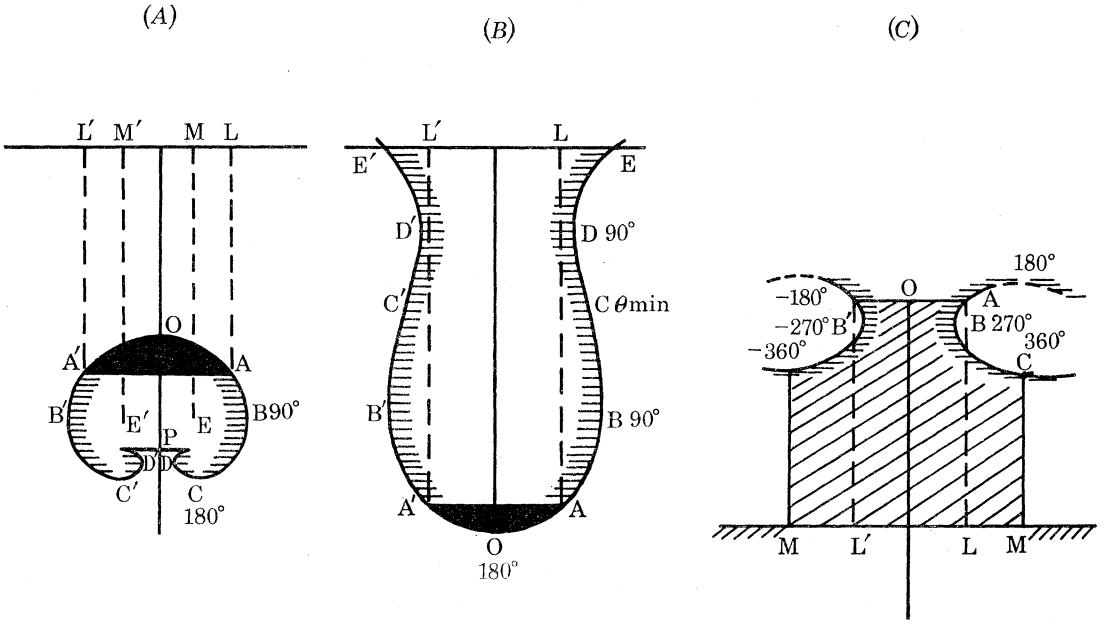

FIGURE 4. The volumes of meniscus profiles supported by surface forces. (*A*) Sessile drop; (*B*) pendant drop; (*C*) liquid bridge.

The volumes, in dimensionless form, swept out by rotating the sessile-drop, pendant-drop and liquid-bridge profiles on their axes of symmetry were integrated and included in the tables. The volume of increments, δV, of closed menisci up to the first 20° were assumed to be the volumes of spherical segments given by

$$\delta V = \pi[R_h(Z^2-(Z-\delta Z)^2)-\tfrac{1}{3}\{Z^3+(Z-\delta Z)^3\}]. \tag{17}$$

However above 20°, volume increments were assumed to be segments of a cone given by

$$\delta V = \pi\delta Z[X^2-X\delta X+\tfrac{1}{3}(\delta X)^2]. \tag{18}$$

Equation (18) was in most cases somewhat too inaccurate to be used for anything more than a general check on the force calculations. It will be seen that for closed menisci the volume represents the total volume of the drop and it equalled the force calculated as a dimensionless volume. That it did not do so sufficiently accurately represented an error due to cumulative underestimates of the volume resulting from the use of equation (18).

The main point to come out from this treatment is that the force acting in a liquid bridge may be represented by a volume of liquid displaced from the free surface. This displaced volume bore no relation to the volume of an axisymmetric liquid bridge between two parallel planes. However, the difference between the forces between those two parallel planes does give the volume of liquid actually forming the bridge.

Tables of meniscus profiles

Examples of the tables of profiles produced in this study are shown in tables 3A, B and C. In all tables the values of X/R_0, Z/R_0, the two principal radii of curvature, R_v/R_0 and R_h/R_0, the volume and the force are shown as a function of the angle ϕ. In table 3A the profile of a distorted nodoid, which is plotted out in figure 3, produces the shape of a sessile drop ($\phi = 0$ to 180°) and a vapour bridge ($\phi = 180$ to 360°). When inverted, this profile produces that of a captive bubble ($\phi = 0$ to 180°) and a liquid bridge ($\phi = 180$ to 360°).

Table 3B shows the corresponding profile properties of a distorted unduloid which in the form presented produces a pendant drop with the same shape factor β as the sessile drop. This is also plotted in figure 3 which, when inverted, becomes the shape of an emergent bubble.

An example of the liquid bridge tables is shown in table 3C. Here the starting conditions differ from those of tables 3A and 3B and are found at $\phi = 270°$. This profile has not been plotted here but others like it are shown and discussed in relation to figure 11.

In all, 190 tables of pendant and sessile-drop profiles have been generated and a further 200 tables for open menisci of the liquid bridge type. A small set of tables has also been generated for the special conditions relating to the profile formed with a rod at a free liquid surface.

Clearly, it is not possible to publish such a wide set of data here, so only the most important features of these profiles will be discussed. They will be discussed in part II, and are presented with the aid of graphs, some of which have been drawn with great accuracy, using an automatic graph plotter with a Hewlett–Packard 9100A computer.

Errors

The tables calculated by this procedure possessed errors of three basic kinds:

(1) Arithmetic errors, arising within the computer, due to calculation with insufficient decimal digits.

(2) Errors due to using a first-order integration method with a second-order equation.

(3) Errors arising at inflexion points on the profile.

Arithmetic errors within the computer were very small when compared with other errors. However, a cumulative arithmetic error arose during the summing of increments of the angle ϕ. This error was always negative and amounted to -8.83×10^{-5} %. This meant that for a nominal angle of 360° the true computed angle was 359° 59′ 59″. This is not serious and is well below experimental error.

The second type of error arose mainly because the assumption that R_v is invariant over a very small increment is of course incorrect. Thus the calculated values of δX and δZ according to equations (10) and (11) also possess an error. An estimate of this error was made by calculating the values of X/b, Z/b, R_v/b and R_h/b with different increments of $\delta\phi$. These results are seen in table 4 and indicate that when $\delta\phi = 0.02°$ the general error was no greater than $\pm 1 \times 10^{-3}$ % in any of these terms. In general one may regard four figures of decimal of the values tabulated as correct but should take at least five figures for interpolation. In table 5 a slightly wider comparison of the figures of Bashforth & Adams is made with the corresponding figures of this study for an increment $\delta\phi = 0.02°$.

The very wide set of data obtained in this study has enabled comparisons with many other published data and in all cases the errors have been no greater than those recorded above except for the conditions of a change in gradient in the profile.

PHILOSOPHICAL TRANSACTIONS OF THE ROYAL SOCIETY A MATHEMATICAL, PHYSICAL & ENGINEERING SCIENCES

TABLE 3A. DISTORTED NODOID (SESSILE DROP/CAPTIVE BUBBLE) PROFILE

solutions of the meniscus equation $\beta = 0.5000$

angle $\pm\phi$	$\pm X/b$	Z/b	vert. radius, R_v/b	horiz. radius, R_h/b	volume, V/b^3	force, $F/\rho g b^3$
0	0.000000	0.000000	1.000000	1.000000	0.000000	0.000000
5	0.087114	0.003802	0.998573	0.999527	0.000045	0.000045
10	0.173321	0.015149	0.994342	0.998119	0.000716	0.000718
15	0.257736	0.033859	0.987429	0.995818	0.003550	0.003560
20	0.339520	0.059639	0.978034	0.992692	0.010897	0.010934
25	0.417898	0.092096	0.966412	0.988833	0.025698	0.025744
30	0.492174	0.130752	0.952856	0.984349	0.051045	0.051104
35	0.561740	0.175059	0.937682	0.979364	0.089917	0.089991
40	0.626083	0.224418	0.921209	0.974013	0.144846	0.144938
45	0.684787	0.278195	0.903746	0.968435	0.217663	0.217774
50	0.737530	0.335737	0.885577	0.962777	0.309328	0.309460
55	0.784079	0.396381	0.866956	0.957184	0.419843	0.419996
60	0.824286	0.459472	0.848103	0.951804	0.548258	0.548431
65	0.858081	0.524366	0.829200	0.946788	0.692739	0.692931
70	0.885462	0.590437	0.810389	0.942289	0.850706	0.850913
75	0.906489	0.657086	0.791781	0.938466	1.019001	1.019221
80	0.921277	0.723740	0.773447	0.935490	1.194087	1.194317
85	0.929993	0.789858	0.755432	0.933546	1.372247	1.372482
90	0.932846	0.854927	0.737748	0.932846	1.549773	1.550009
95	0.930083	0.918471	0.720381	0.933635	1.723147	1.723382
100	0.921988	0.980042	0.703291	0.936211	1.889187	1.889416
105	0.908878	1.039227	0.686414	0.940939	2.045160	2.045380
110	0.891100	1.095645	0.669661	0.948289	2.188874	2.189080
115	0.869032	1.148951	0.652919	0.958870	2.318719	2.318908
120	0.843078	1.198831	0.636052	0.973502	2.433689	2.433855
125	0.813672	1.245009	0.618900	0.993309	2.533362	2.533503
130	0.781277	1.287247	0.601279	1.019883	2.617865	2.617977
135	0.746380	1.325347	0.582991	1.055539	2.687805	2.687882
140	0.709500	1.359158	0.563823	1.103783	2.744186	2.744225
145	0.671176	1.388581	0.543565	1.170157	2.788323	2.788318
150	0.631971	1.413574	0.522027	1.263938	2.821731	2.821679
155	0.592458	1.434159	0.499065	1.401869	2.846035	2.845930
160	0.553212	1.450433	0.474615	1.617474	2.862864	2.862702
165	0.514791	1.462564	0.448729	1.988985	2.873776	2.873553
170	0.477719	1.470800	0.421602	2.751040	2.880184	2.879895
175	0.442458	1.475460	0.393585	5.076501	2.883311	2.882954
180	0.409388	1.476922	0.365169	162889.321166	2.884165	2.883739
185	0.378790	1.475604	0.336940	−4.346258	2.883539	2.883044
190	0.350834	1.471941	0.309509	−2.020406	2.882020	2.881458
195	0.325587	1.466361	0.283438	−1.257984	2.880025	2.879399
200	0.303019	1.459262	0.259179	−0.885975	2.877829	2.877145
205	0.283027	1.450997	0.237040	−0.669705	2.875605	2.874868
210	0.265459	1.441866	0.217181	−0.530922	2.873452	2.872668
215	0.250131	1.432114	0.199634	−0.436092	2.871419	2.870596
220	0.236848	1.421934	0.184335	−0.368472	2.869526	2.868669
225	0.225419	1.411473	0.171157	−0.318792	2.867773	2.866888
230	0.215665	1.400838	0.159938	−0.281531	2.866150	2.865243
235	0.207423	1.390108	0.150506	−0.253217	2.864643	2.863719
240	0.200552	1.379332	0.142697	−0.231578	2.863236	2.862299

PHILOSOPHICAL TRANSACTIONS OF THE ROYAL SOCIETY A MATHEMATICAL, PHYSICAL & ENGINEERING SCIENCES

TABLE 3A (*cont.*)

angle $\pm\phi$	$\pm X/b$	Z/b	vert. radius, R_v/b	horiz. radius, R_h/b	volume, V/b^3	force, $F/\rho g b^3$
245	0.194932	1.368545	0.136358	−0.215084	2.861912	2.860966
250	0.190464	1.357766	0.131361	−0.202688	2.860656	2.859704
255	0.187067	1.347001	0.127599	−0.193666	2.859452	2.858497
260	0.184683	1.336253	0.124991	−0.187532	2.858287	2.857330
265	0.183268	1.325515	0.123480	−0.183968	2.857146	2.856188
270	0.182799	1.314780	0.123033	−0.182799	2.856018	2.855060
275	0.183268	1.304038	0.123644	−0.183968	2.854888	2.853930
280	0.184686	1.293280	0.125329	−0.187535	2.853746	2.852786
285	0.187078	1.282495	0.128131	−0.193677	2.852576	2.851614
290	0.190491	1.271678	0.132120	−0.202716	2.851366	2.850400
295	0.194989	1.260828	0.137392	−0.215146	2.850102	2.849128
300	0.200656	1.249951	0.144072	−0.231698	2.848766	2.847782
305	0.207600	1.239062	0.152314	−0.253432	2.847342	2.846344
310	0.215950	1.228190	0.162300	−0.281901	2.845812	2.844796
315	0.225861	1.217385	0.174233	−0.319414	2.844158	2.843118
320	0.237513	1.206720	0.188334	−0.369503	2.842362	2.841292
325	0.251108	1.196302	0.204819	−0.437791	2.840411	2.839306
330	0.266866	1.186277	0.223876	−0.533729	2.838302	2.837154
335	0.285017	1.176844	0.245626	−0.674402	2.836050	2.834851
340	0.305784	1.168259	0.270077	−0.894040	2.833703	2.832447
345	0.329361	1.160843	0.297065	−1.272530	2.831361	2.830041
350	0.355889	1.154980	0.326218	−2.049426	2.829210	2.827821
355	0.385421	1.151112	0.356926	−4.421948	2.827554	2.826092
360	0.417893	1.149714	0.388369	−76460.809631	2.826865	2.825328

TABLE 3B. DISTORTED UNDULOID (PENDANT DROP/EMERGENT BUBBLE) PROFILE

solutions of the meniscus equation $\beta = +0.5000$

angle ϕ	angle $180-\phi$	$\pm X/b$	Z/b	vert. radius, R_v/b	horiz. radius, R_h/b	volume, V/b^3	force, $F/\rho g b^3$
180	0	0.000000	−0.000000	1.000000	1.000000	0.000000	0.000000
175	5	0.087197	−0.003808	1.001432	1.000474	0.000045	0.000045
170	10	0.173978	−0.015235	1.005754	1.001899	0.000726	0.000727
165	15	0.259926	−0.034294	1.013056	1.004277	0.003663	0.003662
160	20	0.344621	−0.061005	1.023493	1.007606	0.011513	0.011496
155	25	0.427640	−0.095402	1.037298	1.011883	0.027829	0.027822
150	30	0.508552	−0.137535	1.054797	1.017104	0.057082	0.057091
145	35	0.586918	−0.187476	1.076432	1.023261	0.104450	0.104479
140	40	0.662289	−0.245331	1.102803	1.030339	0.175702	0.175758
135	45	0.734196	−0.311250	1.134722	1.038311	0.277060	0.277149
130	50	0.802153	−0.385447	1.173308	1.047136	0.415055	0.415182
125	55	0.865638	−0.468232	1.220127	1.056749	0.596409	0.596580
120	60	0.924090	−0.560051	1.277449	1.067048	0.827969	0.828189
115	65	0.976884	−0.661564	1.348682	1.077872	1.116725	1.116998
110	70	1.023298	−0.773767	1.439224	1.088971	1.470023	1.470351
105	75	1.062460	−0.898223	1.558245	1.099939	1.896126	1.896510
100	80	1.093237	−1.037530	1.722899	1.110102	2.405604	2.406039
95	85	1.113996	−1.196404	1.970270	1.118251	3.014827	3.015304
90	90	1.121951	−1.384818	2.402188	1.121951	3.756469	3.756966
85	95	1.110511	−1.631772	3.483658	1.114753	4.726262	4.726714
80.860	99.140	0.999111	−2.400276	−5.310117	1.011959	7.436129	7.379044
90	90	0.956438	−2.866661	−2.088222	0.956438	8.819217	8.761918

PHILOSOPHICAL TRANSACTIONS OF THE ROYAL SOCIETY A MATHEMATICAL, PHYSICAL & ENGINEERING SCIENCES

TABLE 3B (*cont.*)

angle ϕ	angle $180-\phi$	$\pm X/b$	Z/b	vert. radius, R_v/b	horiz. radius, R_h/b	volume, V/b^3	force, $F/\rho g b^3$
95	85	0.963626	−3.035232	−1.813518	0.967307	9.306065	9.248778
100	80	0.983360	−3.185762	−1.682502	0.998530	9.753220	9.695953
105	75	1.014467	−3.326245	−1.625295	1.050254	10.192693	10.135441
110	70	1.056870	−3.460751	−1.614196	1.124698	10.645062	10.587813
115	65	1.111048	−3.391513	−1.635377	1.225906	11.126846	11.069584
120	60	1.177783	−3.719649	−1.680318	1.359988	11.653119	11.595825
125	55	1.257974	−3.845450	−1.742487	1.535704	12.238288	12.180940
130	50	1.352457	−3.968505	−1.815996	1.765508	12.895731	12.838311
135	45	1.461837	−4.087798	−1.895340	2.067351	13.636490	13.578977
140	40	1.586361	−4.201833	−1.975844	2.467940	14.467146	14.409528
145	35	1.725867	−4.308816	−2.054446	3.008958	15.387176	15.329441
150	30	1.879846	−4.406855	−2.130349	3.759694	16.386124	16.328263
155	25	2.047601	−4.494128	−2.205261	4.845038	17.440851	17.382853
160	20	2.228451	−4.568985	−2.283253	6.515557	18.541551	18.454593
165	15	2.421964	−4.629941	−2.370601	9.357753	—	19.485988
170	10	2.628191	−4.675591	−2.476061	15.135151	—	20.395529
175	5	2.847947	−4.704435	−2.612187	32.676528	—	21.068778

TABLE 3C. LIQUID BRIDGE PROFILE

solution of meniscus equation for the liquid bridge $\beta = 0.100000$. $R_v(270°) = -0.300000$

angle ϕ	$\pm X/R_h(270°)$	$Z/R_h(270°)$	vert. radius $R_v/R_h(270°)$	horiz. radius R_h/R_h (270°)	volume $V/R_h(270°)^3$	force $F/\rho g R_h(270°)^3$
0	1.338170	0.750395	−0.442812	−330236.943481	−127.054822	−127.043443
5	1.377321	0.748678	−0.455542	−15.802265	−127.064858	−127.053886
10	1.417267	0.743411	−0.468062	−8.161530	−127.097263	−127.086688
15	1.457654	0.734449	−0.480231	−5.631858	−127.155546	−127.145351
20	1.498099	0.721689	−0.491917	−4.380101	−127.243222	−127.233383
25	1.538197	0.705072	−0.502999	−3.639653	−127.363669	−127.354157
30	1.577524	0.684592	−0.513368	−3.155027	−127.519959	−127.510740
35	1.615651	0.660295	−0.522933	−2.816786	−127.714685	−127.705723
40	1.652147	0.632283	−0.531620	−2.570273	−127.949778	−127.941034
45	1.686592	0.600713	−0.539371	−2.385193	−128.226338	−128.217779
50	1.718583	0.565794	−0.546146	−2.243445	−128.544510	−128.536099
55	1.747743	0.527786	−0.551918	−2.133595	−128.903363	−128.895066
60	1.773726	0.486994	−0.556674	−2.048119	−129.300838	−129.292619
65	1.796227	0 443765	−0.560414	−1.981914	−129.733730	−129.725565
70	1.814983	0.398479	−0.563144	−1.931463	−130.197749	−130.189613
75	1.829780	0.351545	−0.564880	−1.894326	−130.687621	−130.679498
80	1.840454	0.303394	−0.565641	−1.868845	−131.197238	−131.189111
85	1.846895	0.254472	−0.565451	−1.853949	−131.719854	−131.711716
90	1.849045	0.205232	−0.564337	−1.849045	−132.248319	−132.240170
95	1.846902	0.156128	−0.562324	−1.853958	−132.775319	−132.767211
100	1.840517	0.107610	−0.559440	−1.868910	−133.293635	−133.285577
105	1.829990	0.060116	−0.555712	−1.894546	−133.796382	−133.788392
110	1.815472	0.014063	−0.551169	−1.931987	−134.277234	−134.269334
115	1.797162	−0.030150	−0.545836	−1.982951	−134.730619	−134.722832
120	1.775299	−0.072157	−0.539743	−2.049941	−135.151861	−135.144214
125	1.750160	−0.111624	−0.532920	−2.136555	−135.537291	−135.529816
130	1.722060	−0.148254	−0.525398	−2.247994	−135.884297	−135.877024
135	1.691337	−0.181790	−0.517213	−2.391917	−136.191336	−136.184299
140	1.658355	−0.212019	−0.508406	−2.579949	−136.457882	−136.451117
145	1.623494	−0.238776	−0.499023	−2.830485	−136.684363	−136.677903
150	1.587144	−0.261941	−0.489117	−3.174300	−136.872037	−136.865912

PHILOSOPHICAL TRANSACTIONS OF THE ROYAL SOCIETY A MATHEMATICAL, PHYSICAL & ENGINEERING SCIENCES

TABLE 3c (*cont.*)

angle $\pm\phi$	$\pm X/R_h(270°)$	$Z/R_h(270°)$	vert. radius, $R_v/R_h(270°)$	horiz. radius, $R_h/R_h(270°)$	volume, $V/R_h(270°)^3$	force, $F/\rho g R_h(270°)^3$
155	1.549698	−0.281442	−0.478750	−3.666915	−137.022859	−137.017099
160	1.511548	−0.297252	−0.467992	−4.419493	−137.139333	−137.133962
165	1.473073	−0.309390	−0.456918	−5.691557	−137.224357	−137.219398
170	1.434641	−0.317917	−0.445615	−8.261848	−137.281075	−137.276545
175	1.396595	−0.322933	−0.434174	−16.024438	−137.312736	−137.308645
180	1.359258	−0.324571	−0.422491	883214.459716	−137.322576	−137.318929
185	1.322918	−0.322992	−0.411266	15.178535	−137.313748	−137.310511
190	1.287837	−0.318380	−0.399998	7.416300	−137.289149	−137.286316
195	1.254240	−0.310939	−0.388986	4.845989	−137.251464	−137.249018
200	1.222322	−0.300882	−0.378324	3.573820	−137.203095	−137.201018
205	1.192244	−0.288431	−0.368100	2.821084	−137.146150	−137.144417
210	1.164138	−0.273806	−0.358395	2.328272	−137.082439	−137.081022
215	1.138106	−0.257229	−0.349280	1.984225	−137.013492	−137.012358
220	1.114227	−0.238913	−0.340818	1.733428	−136.940571	−136.939687
225	1.092557	−0.219062	−0.333062	1.545108	−136.864703	−136.864034
230	1.073135	−0.197873	−0.326055	1.400878	−136.786703	−136.786214
235	1.055985	−0.175530	−0.319835	1.289120	−136.707205	−136.706862
240	1.041121	−0.152204	−0.314428	1.202183	−136.626686	−136.626458
245	1.028548	−0.128057	−0.309857	1.134877	−136.545499	−136.545357
250	1.018266	−0.103241	−0.306138	1.083616	−136.463890	−136.463808
255	1.010273	−0.077895	−0.303285	1.045912	−136.382024	−136.381980
260	1.004566	−0.052155	−0.301306	1.020063	−136.300002	−136.299980
265	1.001141	−0.026149	−0.300209	1.004965	−136.217879	−136.217870
270	1.000000	0.000000	−0.300000	1.000000	−136.135681	−136.135681
275	1.001142	0.026169	−0.300681	1.004967	−136.053419	−136.053380
280	1.004575	0.052237	−0.302258	1.020072	−135.971101	−135.971016
285	1.010306	0.078079	−0.304729	1.045945	−135.888757	−135.888607
290	1.018344	0.103565	−0.308095	1.083699	−135.806427	−135.806200
295	1.028700	0.128561	−0.312353	1.135045	−135.724211	−135.723886
300	1.041385	0.152923	−0.317495	1.202488	−135.642269	−135.641819
305	1.056408	0.176496	−0.323509	1.289635	−135.560843	−135.560238
310	1.073770	0.199115	−0.330377	1.401706	−135.480282	−135.479490
315	1.093467	0.220604	−0.338073	1.546394	−135.401067	−135.400052
320	1.115482	0.240771	−0.346560	1.735381	−135.323839	−135.322565
325	1.139786	0.259412	−0.355792	1.987154	−135.249432	−135.247861
330	1.166326	0.276313	−0.365711	2.332650	−135.178903	−135.177001
335	1.195031	0.291248	−0.376243	2.827678	−135.113565	−135.111298
340	1.225799	0.303985	−0.387303	3.583985	−135.055014	−135.052352
345	1.258498	0.314287	−0.398793	4.862444	−135.005154	−135.002075
350	1.292964	0.321921	−0.410602	7.445934	−134.966211	−134.962695
355	1.328995	0.326657	−0.422609	15.248285	−134.940732	−134.936767
360	1.366353	0.328280	−0.434686	968870.832519	−134.931569	−134.927151

PHILOSOPHICAL TRANSACTIONS OF THE ROYAL SOCIETY A MATHEMATICAL, PHYSICAL & ENGINEERING SCIENCES

Errors were also sought by carrying out the integration process for a given profile from 0 to 360°, and then returning with a negative increment back to zero. Agreement between the forward and backward integration was within the above errors except in the backward process from 10 to 0°; then it appeared that forward integration was always more accurate when R_v was decreasing as in the case of sessile-drop profiles.

TABLE 4. ESTIMATION OF ERRORS

starting conditions: $\beta = 1.0$ $R_v = R_h = b = 1.0$ at $\phi = 0$

values for $\phi = 90°$

$\delta\phi$	X/b	Z/b	R_v/b	R_h/b	computation time
		calculated to 12 digits of which 7 displayed			
5	0.8912161	0.7734379	0.6055558	0.8912161	20 s
1	0.8864929	0.7680224	0.6097629	0.8864929	2 min
0.5	0.8858929	0.7673643	0.6102921	0.8858929	4 min
0.2	0.8855318	0.7669714	0.6106100	0.8855318	9 min
0.1	0.8854113	0.7668408	0.6107160	0.8854113	18 min
0.05	0.8853510	0.7667756	0.6107691	0.8853510	35 min
0.02	0.8853148	0.7667365	0.6108009	0.8853418	1½ h
0.01	0.8853027	0.7667234	0.6108115	0.8853027	3 h
0.005	0.8852967	0.7667169	0.6108168	0.8852967	6 h
	0.88529	0.76671	Bashforth & Adams		

TABLE 5. COMPARISON WITH BASHFORTH & ADAMS

β	ϕ	X/b	Z/b		V/b^3
1.0	10°	0.17300	0.01511	B. & A.	0.00071
		0.172998	0.015106	this study	0.000713
	90°	0.88529	0.76671	B. & A.	1.24972
		0.885314	0.766735	this study	1.249998
	180°	0.46853	1.26459	B. & A.	2.25138
		0.468529	1.264630	this study	2.251417
100	10°	0.13796	0.01079	B. & A.	0.000336
		0.138002	0.010791	this study	0.000336
	90°	0.31646	0.14487	B. & A.	0.031987
		0.316515	0.144877	this study	0.032004
	180°	0.26489	0.20431	B. & A.	0.049445
		0.264948	0.204318	this study	0.049469

The pendant-drop profiles were susceptible to errors greater than those with sessile-drop profiles because the integration process was carried out with values of R_v/b increasing to infinity and then changing sign. Thus for β values of 0.15 or less for pendant-drop conditions the precision of the tables was so poor that they had to be recalculated with a smaller increment ($\delta\phi = 0.005$) to avoid large errors in $\delta Z/b$ and $\delta X/b$ obtained when the profile changed its gradient. These errors were always immediately obvious because the calculated force which depended critically on $\delta X/b$ would show a sharp decrease if the integration procedure produced excessive errors. In this event the integrated volume (although itself in slight error) was more accurate than the calculated force. Volume errors, estimated by using equation (18) for a sphere, were less than 10^{-4} %.

The coordinates and principal radii of curvature of these tables were always better than ± 0.1 % and these errors are certainly less than those likely to be found by experiment.

3. The shape properties of axisymmetric surface profiles

Axisymmetric profiles of liquid surfaces are essentially of two main types, those that are closed and cross the axis of symmetry and those that are open and never cross the axis of symmetry. The former type includes the sessile and pendant drops and their inverse shapes, the

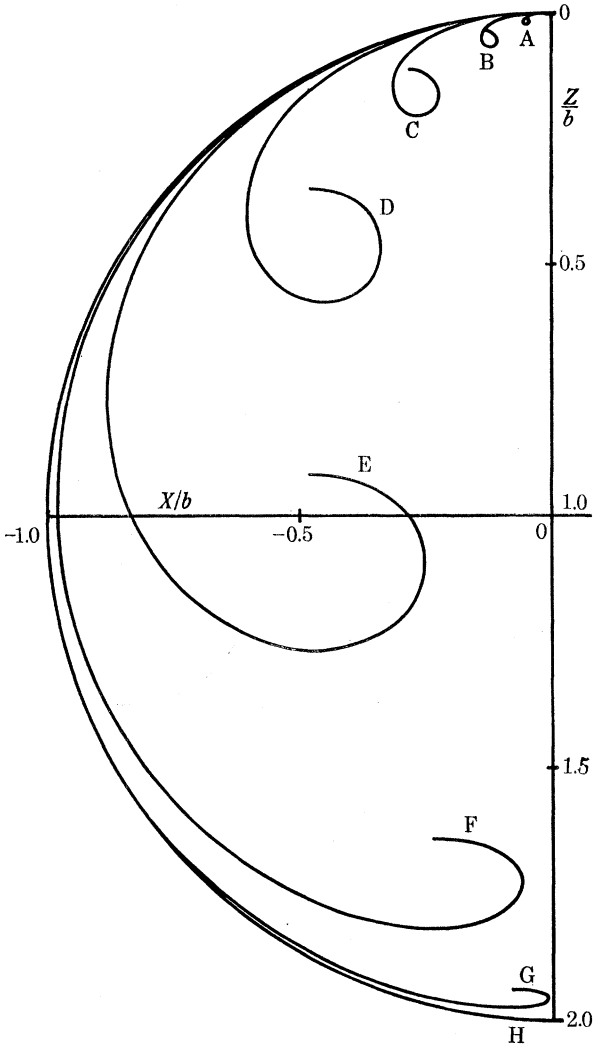

Figure 5. Sessile drop profiles. Values of β: A, 10^4; B, 10^3; C, 10^2; D, 10; E, 1; F, 10^{-1}; G, 10^{-2}; H, 0.

emergent and captive bubbles, whilst the latter include the rod-in-free-surface, many types of liquid bridges and the hole-in-liquid produced in a thin layer of liquid at a horizontal solid surface of low wettability. The general properties of some of these profiles, derived from the tables computed in the previous section, will now be considered in more detail.

Distorted nodoid profiles (sessile drops and captive bubbles)

The new features of the distorted nodoid profiles of this study are first that Bashforth & Adams's tables have been extended into the liquid bridge region, 180 to 360°, and second that the range of the shape factor β has been extended to include values down to 10^{-6} and up to 10^6. Some

shapes in these extended regions, often obtained experimentally, are shown in figure 5. It may be seen from this figure and from figure 3 that the extent of the distortion from a circular shape depends on the value β.

At small values of β (below 0.1) the profiles between $\phi = 0$ and 130° approximate to a circle. Between $\phi = 210$ and 330° the shape of the corresponding bridge approaches the shape of a catenoid. This is seen more readily in figure 9, below.

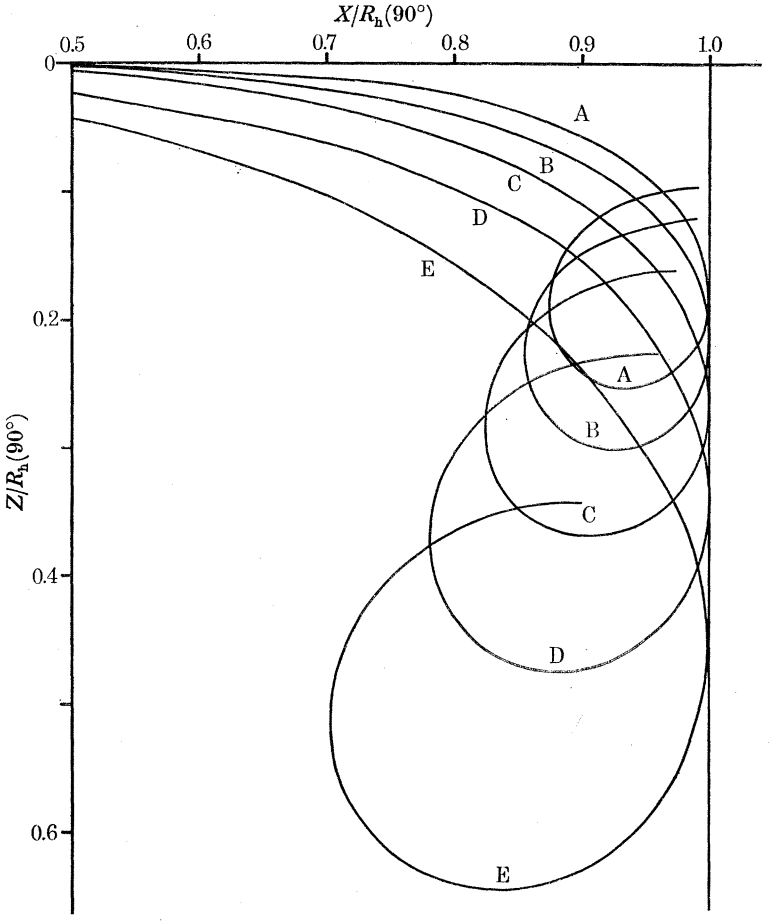

FIGURE 6. Shapes of sections of sessile drop menisci with base altered to $R_h(90°)/b = 1.0$. Values of β: A, 10^6; B, 10^5; C, 10^4; D, 10^3; E, 10^2.

As the value of β increases the distorted nodoid becomes successively more distorted up to a maximum value when $\beta = \infty$. At this point the shape takes the form of a cylindrical profile the shape of which is fully described analytically (Princen 1969). Portions of each of several profiles at large β values are shown in figure 6, but with the base measurement changed to $R_h(90°)/b = 1.0$ so as to magnify the shape changes.

A general feature of all distorted nodoid curves is that the vertical radius of curvature R_v/b must always be positive and must always be less than the corresponding absolute value of R_h/b.

In figure 3 the distorted nodoid curve has been extended over four cycles (of the angle ϕ) and it is seen that the value of $X/b(\text{min})$ for each succeeding cycle increases in value. It was found generally that as each cycle receded from the origin the shape came nearer and nearer to a circle. However, for the first ten cycles, particularly when β was small, curves were of distinctive shape with R_v/b varying over wide limits between 0 and 360° of each cycle.

In figure 7 successive cycles of the profiles of distorted nodoids are shown for large values of β but with the shape inverted in the form of a captive bubble. It will now be seen that the value of X/b (min) for successive bridge conditions (i.e. 270, 630, 990°, etc.) increases much more rapidly and that successive cycles are pulled out and drawn down towards the X/b axis as the value of β increases. Eventually the loop at very high values of β corresponds to that of a cylindrical meniscus.

The bridge conditions of a distorted nodoid profile represent a vapour bridge when forming a part of a sessile drop profile as in figure 3 and a liquid bridge when forming a part of a captive bubble profile as in figure 7. All captive bubble profiles must exist above the free liquid level when the pressure inside them is less than atmospheric.

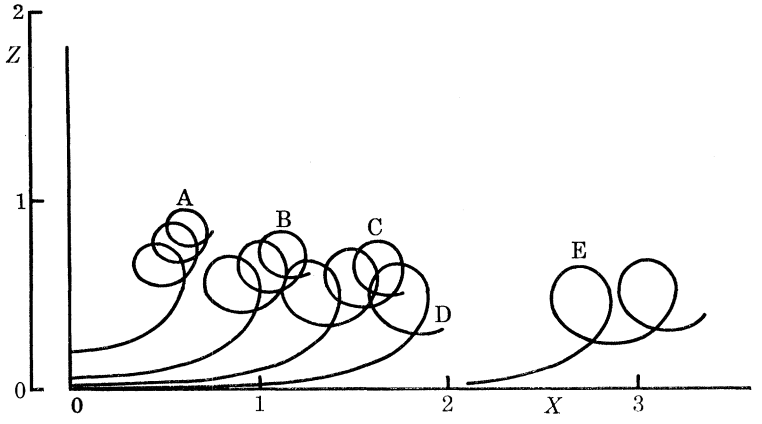

FIGURE 7. Successive cycles of the profiles of captive bubbles for large β values.

	A	B	C	D	E
b	1	$\sqrt{10}$	10	$10^{3/2}$	10^2
β	10	10^2	10^3	10^4	10^5

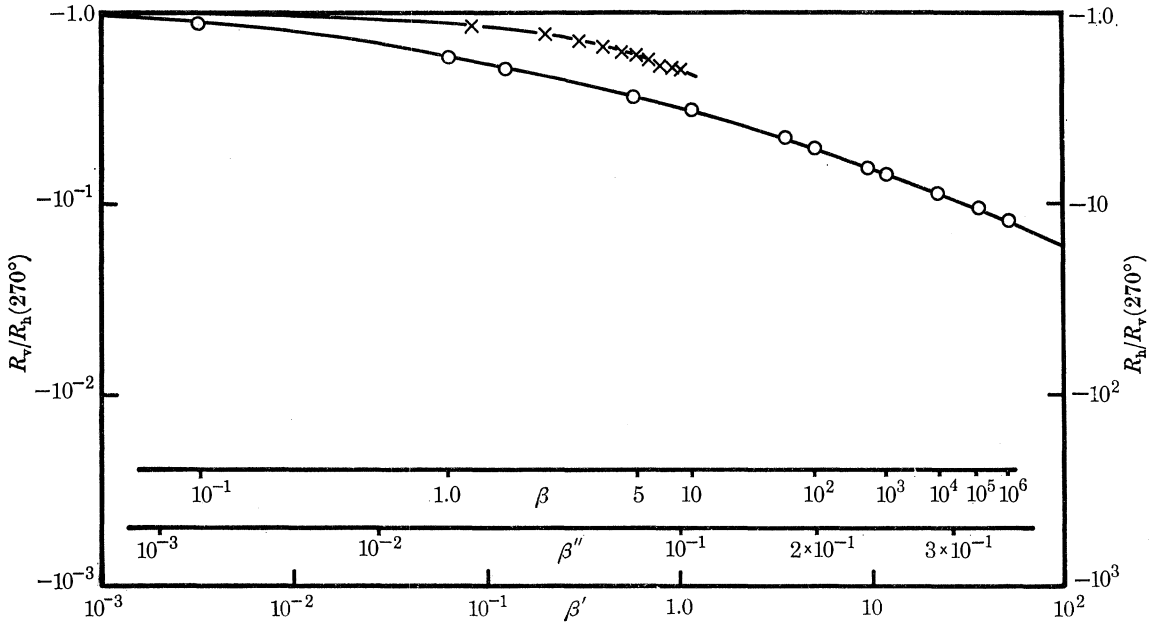

FIGURE 8. Relations between shape factors of axisymmetric menisci: $R_v/R_h(270°)$ as a function of β, β'' or β' for sessile drops (○); and for liquid bridges between a solid and a free liquid surface (×).

For bridge conditions arising from distorted nodoid profiles the ratio R_h/R_v at 270° (or any other defined point on the profile) is sufficient to characterize the shape. These two shape factors are interrelated as shown in figure 8. The shape factor β as defined by Bashforth & Adams is shown as the abscissa on a logarithmic scale in figure 8 together with the logarithm of the two other shape factors defined by table 2. The ordinate of figure 8 is given by the logarithm of the ratio $R_h/R_v(270°)$ or its reciprocal.

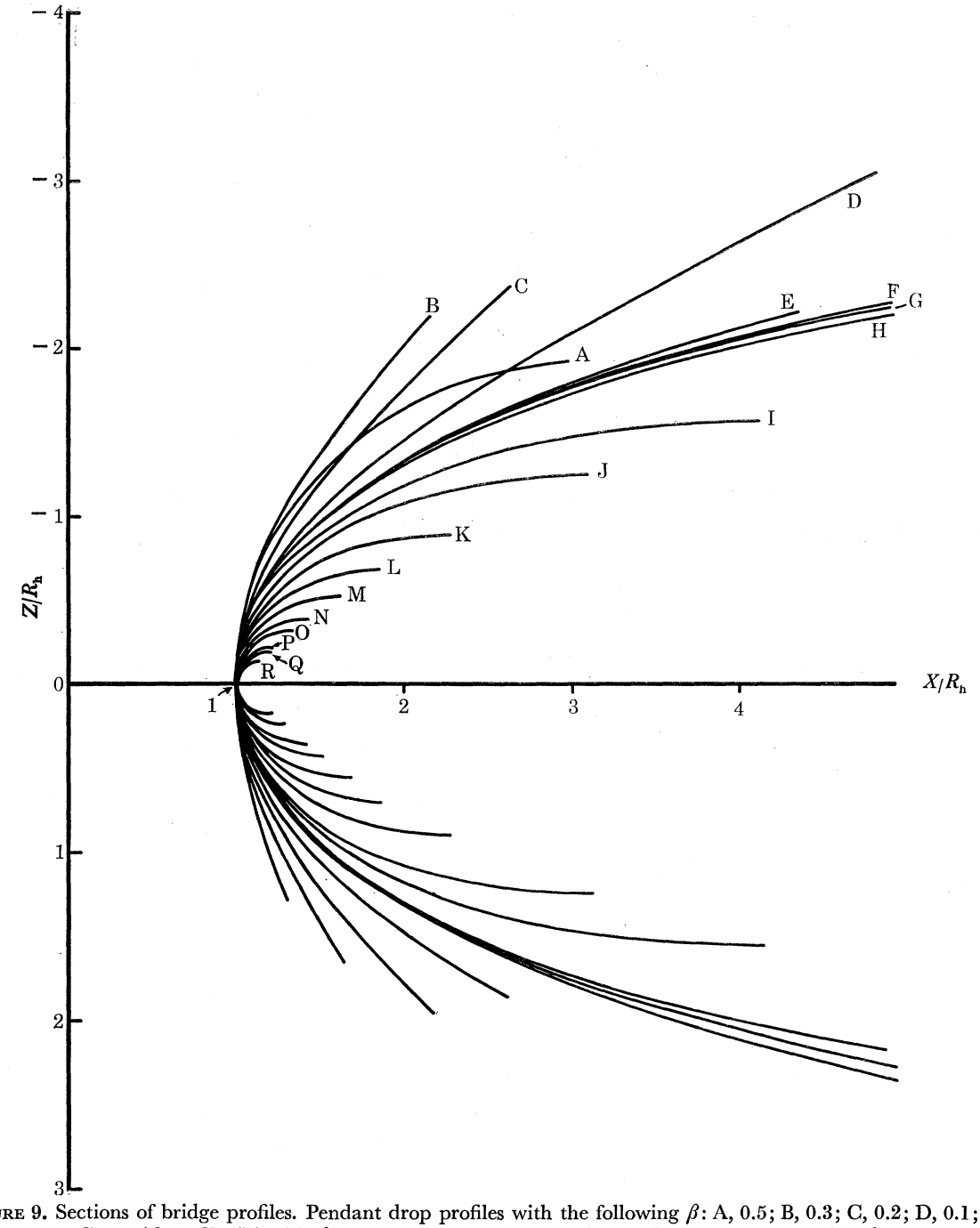

FIGURE 9. Sections of bridge profiles. Pendant drop profiles with the following β: A, 0.5; B, 0.3; C, 0.2; D, 0.1; E, 0.01. Catenoid profile (F) with $\beta = 0.0$. Captive bubble bridge profiles with the following β: G, 0.001; H, 0.01; I, 0.1; J, 0.2; K, 0.5; L, 1; M, 2; N, 5; O, 10; P, 50; Q, 100; R, 1000.

Although a meniscus profile may be constructed with any combination of β and $R_h/R_v(270°)$ only those combinations that fall on the indicated line of figure 8 give rise to closed menisci of the distorted nodoid (sessile-drop) type. Other combinations will most generally generate open menisci as will be described below but, of course, further combinations of R_h/R_v and β can give rise to closed meniscus profiles when they correspond to bridge conditions of the second or subsequent cycles.

The sections of these distorted nodoid profiles that correspond to liquid or vapour bridge conditions possess an important distinguishing feature which is best seen in figure 9. In this figure the base to which all dimensions are related has been converted from b to $R_h(270°)$: so that $R_h(270°)/b = X(270°)/b = 1.0$. The value of $Z/R_h(270°)$ at the value $\phi = 270°$ (i.e. the neck of the bridge) has arbitrarily been taken as the origin so that the bridge shapes may be seen in the form of a nest of curves. The feature of importance is that all these curves obtained from distorted nodoid (sessile-drop) profiles fall inside the shape of a catenoid drawn on the same scale. *It will thus be noted that as the value of β decreases the shape of a liquid bridge derived from a sessile drop becomes nearer and nearer to that of a catenoid* and not, as may be supposed, to that of a circle. However, the implications of this will be discussed more fully under the section dealing with open menisci.

A few of these distorted nodoid shapes were in principle predicted by Lord Kelvin (1886), but the parameters of tables on which his diagrams were based do not appear to have been published at all.

Distorted unduloid profiles (pendant drops and emergent bubbles)

Pendant-drop profiles have been widely used to measure surface tension by the so-called 'pendant-drop method'. This has given rise to several accurate sets of tables for these profiles (Bashforth & Adams 1883; Andreas *et al.* 1938; Fordham 1948; Niederhauser & Bartell 1950; Mills 1953; Stauffer 1965). The tables generated in this study extended these tables to cover the neck or liquid-bridge profiles generated above the first inflexion point on profiles such as that shown in figure 3. This profile possesses only one inflexion point below the free liquid level but for β values lower than 0.3 ($\beta > -0.3$ on Bashforth & Adams scale) the shape possesses more than one inflexion point. Although single cycle unduloid profiles have been published previously (Princen 1969), extensions beyond the first inflexion point, as shown in figure 10, are a new feature and represent greater precision than Lord Kelvin's profiles.

A feature of distorted unduloid profiles that cross the axis of symmetry is the change in sign of the value R_v/b at the inflexion points. Thus after the first change in sign of $\delta\phi$ (from negative to positive because initially ϕ decreases from 180°) the profile, for small values of β, forms a neck which represents a liquid bridge for pendant-drop conditions and a vapour bridge for emergent bubble conditions. Unlike that of liquid bridges derived from captive bubble profiles, the pressure inside the liquid bridge of a pendant drop is always greater than at a free surface.

The shape of the liquid-bridge sections of some of these unduloid profiles may be seen in figure 9. The ratio R_v/R_h at the thinnest part of the neck of these liquid bridges is again negative but is always numerically greater than unity. Thus all these profiles lie outside the shape of the catenoid.

General features of closed menisci

It is thus seen that as a general principle the bridge conditions of closed menisci may be characterized readily by comparison with the shape of a catenoid, distorted unduloid (or pendant-drop) shapes lying outside the catenoid and distorted nodoid (or captive bubble) shapes lying inside the catenoid.

PHILOSOPHICAL TRANSACTIONS OF THE ROYAL SOCIETY A MATHEMATICAL, PHYSICAL & ENGINEERING SCIENCES

The constraint that the profile crosses the axis of symmetry for solutions of equation (4) means that the shape of a profile is completely described either by β or by the ratio R_v/R_h at $\phi 270°$ or some other fixed point.

The shapes of distorted unduloid or distorted nodoid closed menisci can never be adjusted or contrived to fit certain shapes met in practice, such as that of the rod-in-free-surface. It is known from direct experiment that liquid bridge profiles for a given value of β, β', β'' (see table 2)

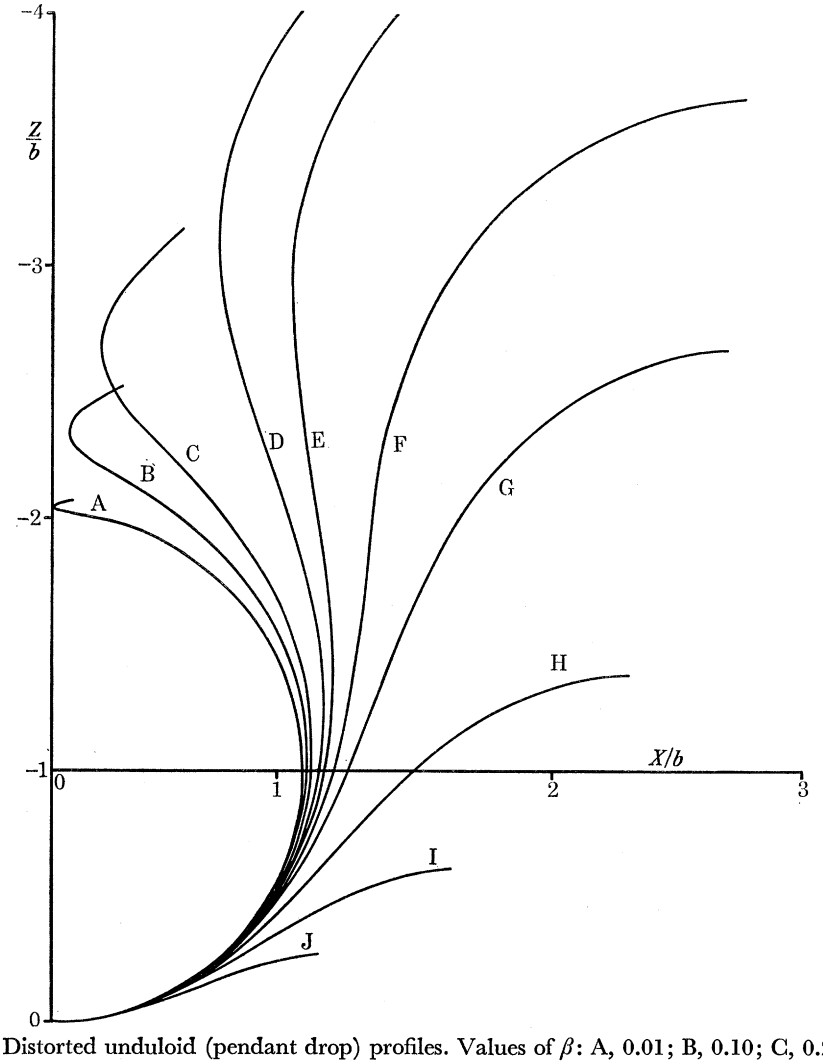

FIGURE 10. Distorted unduloid (pendant drop) profiles. Values of β: A, 0.01; B, 0.10; C, 0.20; D, 0.40; E, 0.50; F, 0.70; G, 1.0; H, 2.0; I, 4.0; J, 10.0.

may vary in shape according to the value of $R_v/R_h(270°)$. This is because many of the shapes actually found corresponded to axisymmetric menisci that never crossed the axis of symmetry. As profiles of this type have special features it will be necessary to consider them separately.

Profiles which do not cross the axis of symmetry (open profiles)

It has been noted already that if the shape factor $\rho g R_0^2/\gamma$ of equation (4) is fixed there are still an infinite number of solutions each of which depends on the starting value of R_h/R_v. As each solution appears to extend infinitely in both directions only a section of each will be considered

in this study and this section is specifically the liquid-bridge profile which forms a part of the whole profile.

In figure 11, the shapes of five open menisci have been obtained for a constant value of $\beta' = \rho g R_h(270°)^2/\gamma$ and with different values of $R_v/R_h(270°)$ varying between -0.7 and -1.0. The starting-point of each curve was adjusted so that the free liquid level of each was positioned at its correct distance above the free liquid surface. All these curves are extensions of profiles which are basically of the captive bubble type.

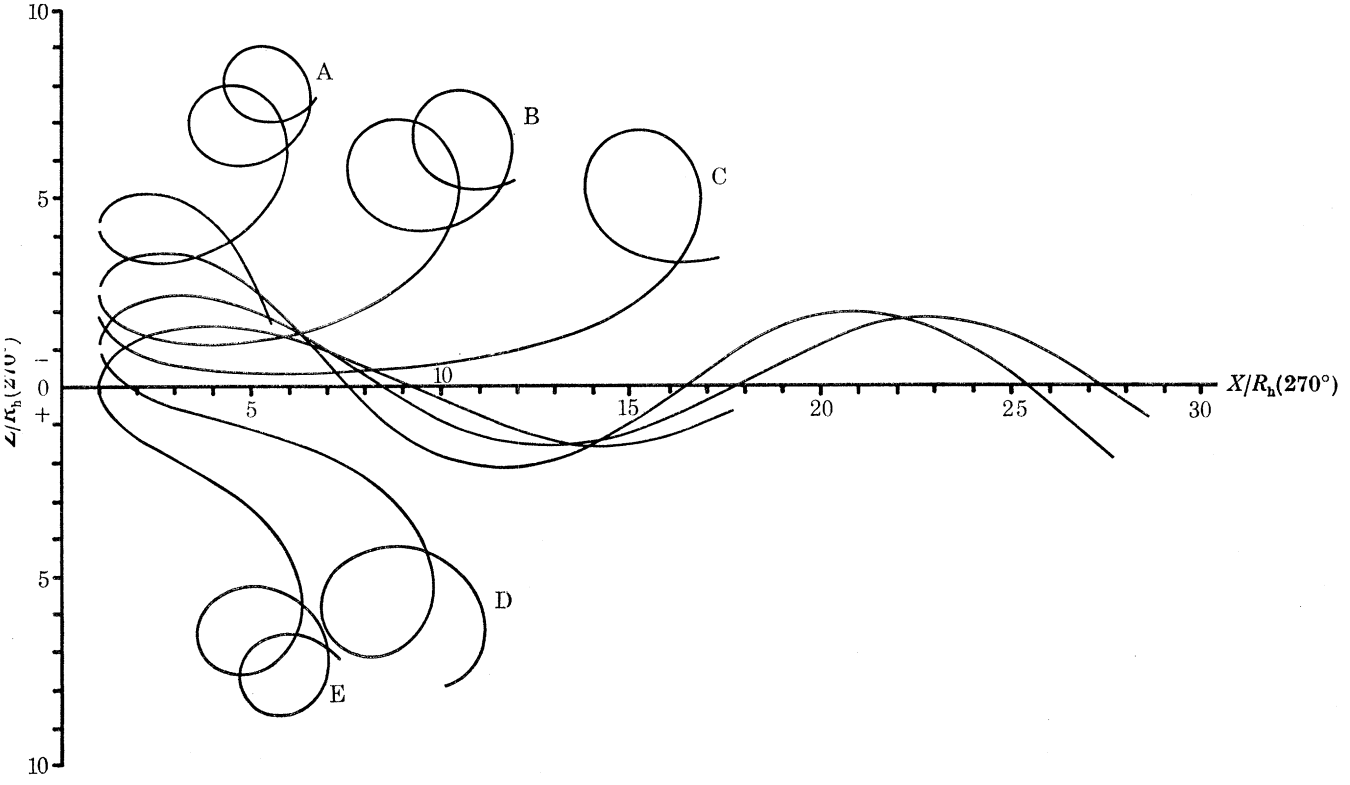

FIGURE 11. Profiles of open menisci over successive cycles. $\beta' = 0.1$. Values of $R_v/R_h(270°)$: A, -0.7; B, -0.8; C, -0.84; D, -0.9; E, -1.0.

Distorted nodoid tables for closed menisci indicate that when $R_v/R_h(270°) = -0.522$ (approx.) and $\beta' = 0.1$ the upper arm of the bridge curve should swing under the starting position and meet the axis of symmetry to form the closed meniscus of a true captive bubble. As the value of R_v/R_h decreases, this upper arm no longer swings under but instead passes through an inflexion point which leads into a horizontal unduloid meniscus which is seen in figure 11. This meniscus corresponds to the improbable condition of rings of liquid hanging from a ceiling.

The lower arm of the liquid-bridge profile given by this method will curve upwards, the real value of R_v being always negative and forming successive cycles of a distorted nodoid, as shown in the figure.

At some point, in this case when $\beta' = 0.1$ and $R_v/R_h = -0.84$ (approx.) the lower arm of the liquid bridge meets the free surface at $\phi = 360°$. For this special condition the value of

$$\{Z(360°) - Z(270°)\}/R_h(270°)$$

must equal the starting value $Z_0/R_h(270°)$ exactly. This condition then gives the profile of a meniscus of a rod-in-free-surface. Such profiles reproduce those obtained in more detail by others (White & Tallmadge 1965; Huh & Scriven 1969). Between $\phi = 350°$ and $360°$ R_v and R_h both became very large as the lower arm of the meniscus approached the free surface asymptotically and this led to errors of the type obtained with pendant-drop profiles where the gradient changed sign.

The condition that the profile just meets the free surface imposes a restraint on solutions of equation (4) which means that a unique set of tables for this condition may be given by defining a single parameter; either the shape factor β' or the starting value $R_v/R_h(270°)$. The relation between β' and $R_v/R_h(270°)$ for the rod-in-free-surface meniscus is shown in figure 8.

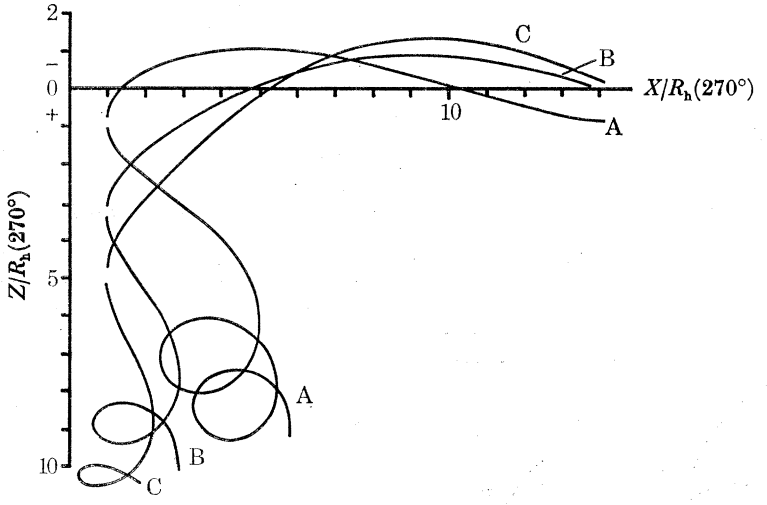

FIGURE 12. Profiles of open menisci over successive cycles. $\beta' = 0.1$. Values of $R_v/R_h(270°)$: A, -1.1; B, -1.5; C, -2.0.

When the value of $R_v/R_h(270°)$ is even smaller than the rod-in-free-surface value the lower arm of the liquid-bridge profile first passes through an inflexion point and then produces distorted nodoids corresponding to vapour bridges of sessile drop menisci. These profiles may be seen in both figures 11 and 12.

In figure 12 the curves of open menisci, again with the same $\beta' = 0.1$ but with lower starting values of $R_v/R_h(270°)$, are shown and it may be seen that the shape of the lower arm of these liquid bridges, although a distorted nodoid below the origin, is beginning to take the form of a pendant drop. In figure 13 further profiles are shown for even lower values of $R_v/R_h(270°)$ within which range the profile passes through the closed shape of the pendant drop. It may be seen that the open menisci pass from a distorted unduloid to a distorted nodoid shape as the profile is generated. This change is accompanied by changes from liquid bridge to vapour bridge profiles.

In curve C of figure 13 the upper arm of the liquid bridge did not form the horizontal unduloids expected. Instead the curve reached some point of greatly reduced pressure and then formed continuous nodoids descending to the origin. It is not yet known if this is a genuine solution of equation (3) or an artefact due to an accumulation of errors. If the former, then it leads to the interesting possibility that all curves are related and are formed from extensions to closed menisci very far from their origin.

Liquid bridges derived from open menisci

In order to compare the shapes of liquid bridges it was found helpful to transfer the base measurement R_0 of equation (4) to the value of $R_v/b(270°)$. This was done merely by dividing all dimensions in tables generated to base b, by the appropriate value of R_v/b at (270°). The shape factor of the new table then becomes β'' of table 2.

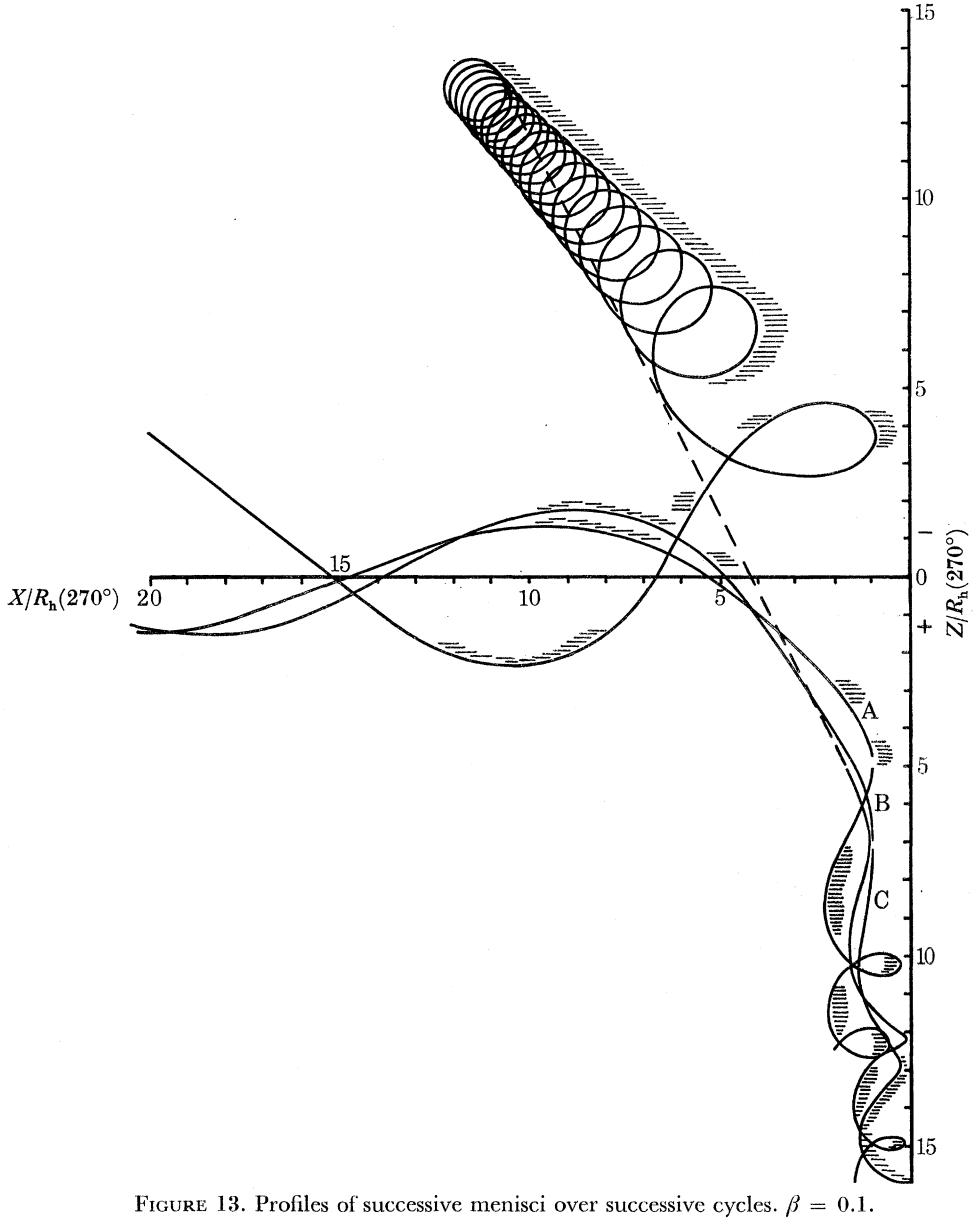

FIGURE 13. Profiles of successive menisci over successive cycles. $\beta = 0.1$.
Values of $R_v/R_h(270°)$: A, −2.0; B, −3.0; C, −4.0.

At small values of β (or β'') it was noted that liquid bridges derived from closed menisci approximated in shape to a catenoid as shown in figure 9. For this special condition it will be seen from figure 8 that the pressures of such menisci are low because the ratio $R_v/R_h(270°)$ very nearly equals −1.0, which implies very low capillary pressure. However, other curves at the same low β'' value

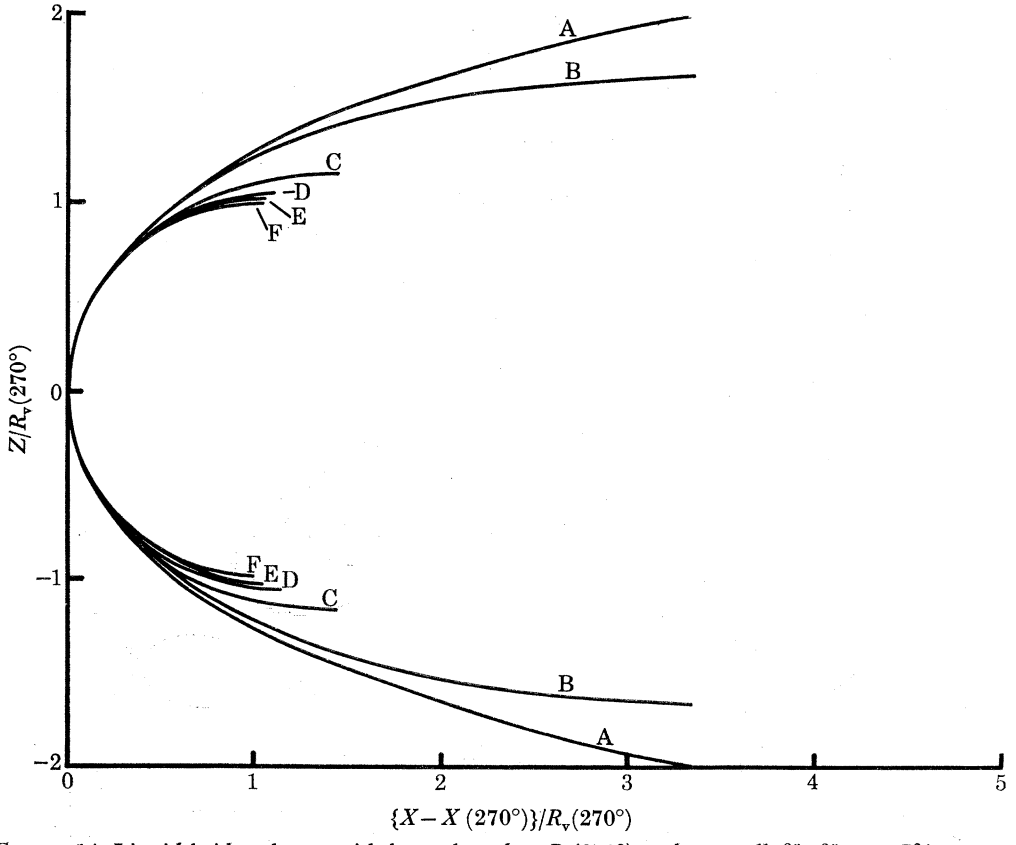

FIGURE 14. Liquid bridge shapes with base altered to $R_v(270°)$ and at small β''. $\beta'' = \rho g R_v^2/\gamma = 10^{-5}$. Values of R_v/R_h: A, -1.0; B, -0.9; C, -0.5; D, -0.2; E, -0.1; F, -0.001.

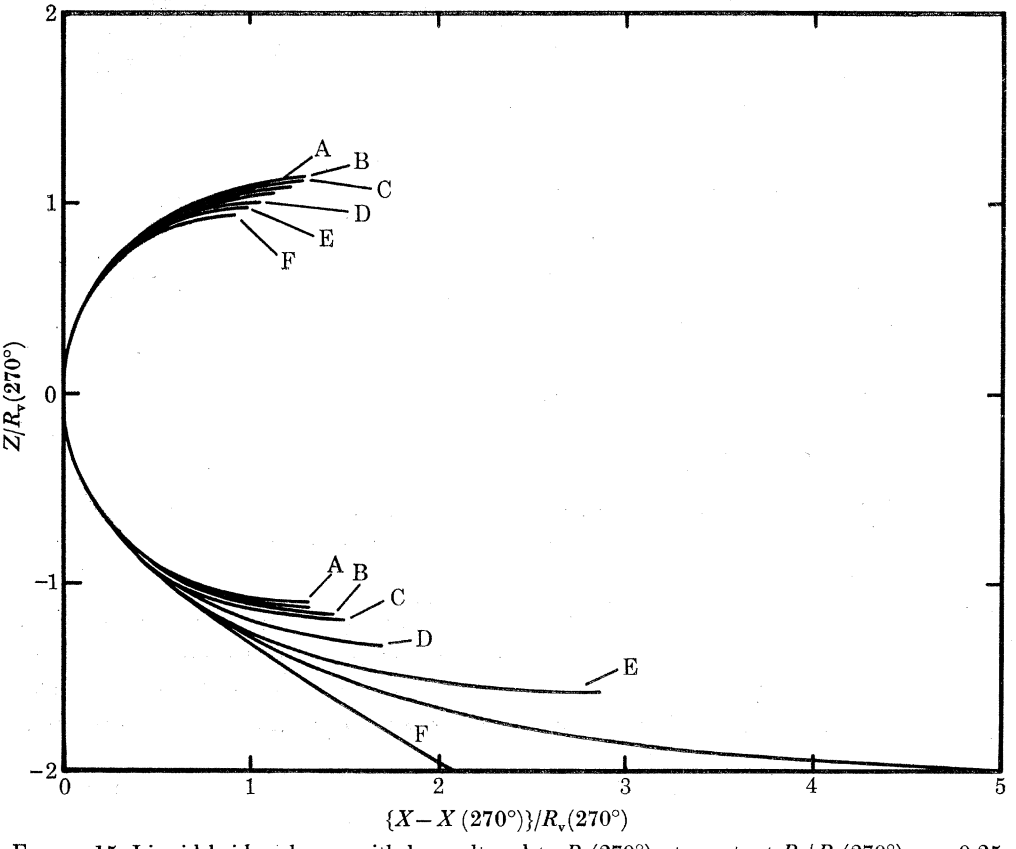

FIGURE 15. Liquid bridge shapes with base altered to $R_v(270°)$ at constant $R_v/R_h(270°) = -0.25$. Values of β'': A, 10^{-3}; B, 10^{-2}; C, 0.12; D, 0.2; E, 0.33; F, 1.0.

may be derived for open menisci, and a selection of such curves is plotted in figure 14, to the base $R_v(270°)$.

An important feature of these profiles is that both arms of each bridge profile are symmetrical. This is because the curve is not distorted by gravity when the value of γ is very large compared with the experimental quantity $\rho g R_v(270°)^2$ or $\rho g R_h(270°)^2$, i.e. β'' is small. A second feature is

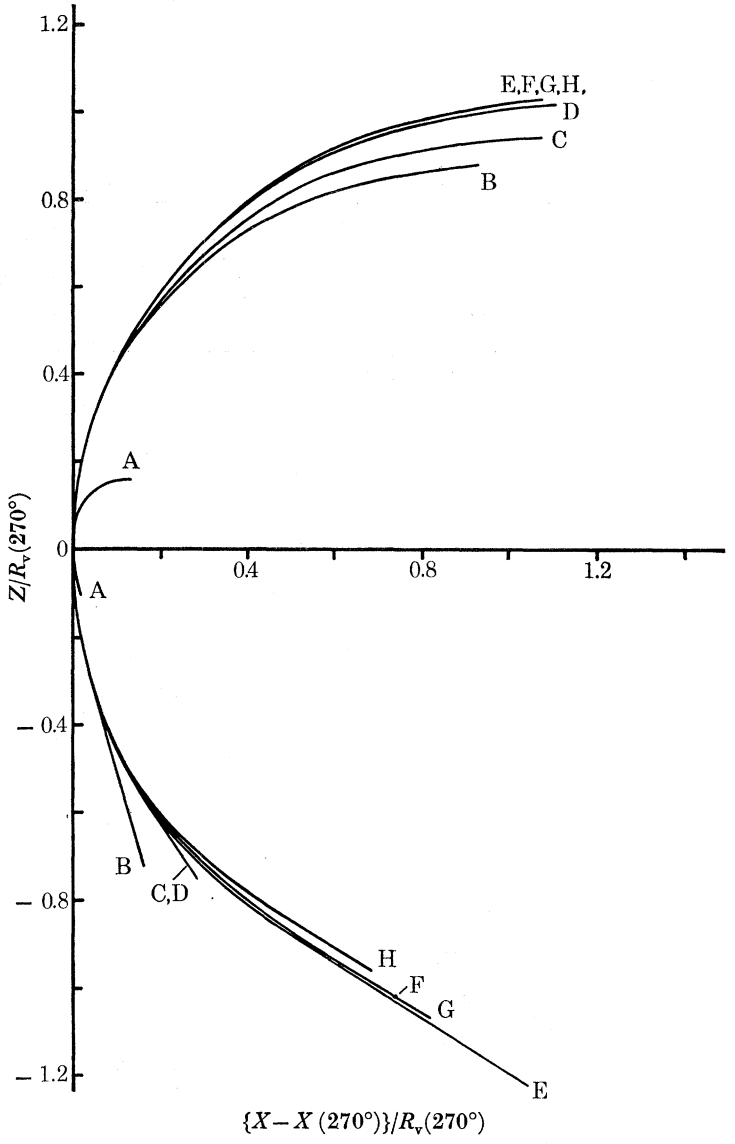

FIGURE 16. Liquid bridge shapes with base altered to $R_v(270°)$ at constant $\beta'' = 1.0$. Values of $R_v/R_h(270°)$: A, -10.0; B, -1.0; C, -0.8; D, $-0{\cdot}5$; E, -0.4; F, -0.3; G, -0.2; H, -0.1.

that the shape changes from that of a catenoid to that of a semicircle as the ratio $R_v/R_h(270°)$ increases from -1.0 to 0. The bridge profile of a meniscus between two spheres or between a sphere and a plate will thus approximate to a circle only when the angle ϕ for liquid/solid contact is within $\pm 30°$ of 270°. Only when this is so will the ratio $R_v/R_h(270°)$ become sufficiently near zero for the profile to approximate to a semicircle.

The effect of changes of β'' (or β' and of $R_v/R_h(270°)$ on the shape of the bridge is seen also in figures 15 and 16.

In figure 15 the shape of the bridge profile is seen to vary with the value β'' at constant ratio $R_v/R_h(270°) = -0.25$. Curve A corresponds to some stage between the catenoid and the circle of figure 14. As β'' increases this has the effect of drawing the upper arm into a circle of diminishing radius and of opening out the lower arm into one of increasing radius in the manner shown. As β'' increases towards a fixed value the profile (approximately curve C) corresponds to that of a closed meniscus. At an even larger value of β'' (curve G) the shape of the profile becomes that of a rod or a sphere at a free surface of liquid.

In figure 16 a further nest of curves has been drawn at a constant value of $\beta'' = 1.0$ for varying values of R_v/R_h. The curves to some extent duplicate the curve of figure 15 but with one important difference: it is now seen that when $R_v/R_h = -0.1$ the shape does not approximate to that of a semicircle. This is because β'' is sufficiently large to produce distinctive distortion of both arms of the liquid bridge. When $R_v/R_h(270°)$ approaches 0 the shape then corresponds to that of a cylindrical meniscus formed between two solid surfaces but is not of the same shape as a cylindrical meniscus formed at a free liquid surface. A cylindrical meniscus at a free surface involves β'' being very large and R_v/R_h being very near to zero, values which are both reached when the experimentally determined quantity $R_h(270°)$ is very large.

This paper, together with the tables it summarizes, is complete in that it covers the shapes of all axisymmetric menisci. The comparison of the profiles with experiment forms a separate study and will be the subject of a further communication.

References

Andreas, J. M., Hauser, E. A. & Tucker, W. B. 1938 *J. phys. Chem.* **42**, 1001.
Bakker, G. 1928 *Handbuch der Experimentalphysik*, **6**. Leipzig: Akademische Verlagsgesellschaft.
Bashforth, F. & Adams, J. C. 1883 *An attempt to test the theories of capillary attraction*. Cambridge University Press.
Blaisdell, B. E. 1940 *J. Math. Phys.* **19**, 186, 217, 220.
Bouasse, H. 1924 *Capillarité Phénomènes Superficiels*. Paris: Libraire Delagrave.
Buff, F. P. 1960 *Handb. Phys.* **10**, 281–304.
Clark, W. C., Haynes, J. M. & Mason, G. 1968 *Chem. Engng Sci.* **23**, 810.
Cross, N. L. & Picknett, R. G. 1963 *Trans. Faraday Soc.* **59**, 846.
Cross, N. L. & Picknett, R. G. 1968 *J. Coll. Interface Sci.* **26**, 247.
Derjaguin, B. V. 1946 *Dokl. Akad. Nauk. SSSR*, **51**, 519.
Derjaguin, B. V. 1968 *J. Coll. Interface Sci.* **26**, 253.
Fisher, R. A. 1926 *J. agric. Sci.* **16**, 492.
Fordham, S. 1948 *Proc. Roy. Soc. Lond.* A **194**, 1.
Gillespie, T. & Rose, G. D. 1968 *J. Coll. Interface Sci.* **26**, 246.
Huh, C. & Scriven, L. E. 1969 *J. Coll. Interface Sci.* **30**, 323.
Kelvin, Lord (Sir W. Thomson) 1886 *Popular lectures and addresses, I*, pp. 1–72. London: The Royal Institution.
Ku, T. C., Ramsey, J. H. & Clinton, W. C. 1968 *I.B.M. Jnl Res. and Dev.* Nov., p. 441.
Laplace, P. S. de 1805 *Mechanique Celeste, suppl. au X libre*. Paris: Coureier.
Mcfarlane, J. S. & Tabor, D. 1950 *Proc. Roy. Soc. Lond.*, A **202**, 224.
Mason, G. & Clark, W. C. 1965 *Chem. Engng Sci.* **20**, 859.
Melrose, J. C. 1966 *A.I.Ch.E. Jl*, **12**, 986–994.
Mills, O. S. 1953 *Br. J. appl. Phys.* **4**, 247.
Niederhauser, D. O. & Bartell, F. E. 1950 *Report of progress—fundamental research on occurrence and recovery of petroleum, 1948–1949*, p. 114. Amer. Pet. Inst., Baltimore.
Nutt, C. W. 1960 *Chem. Engng Sci.* **12**, 133.
Padday, J. F. 1963 *Nature, Lond.* **198**, 378.
Padday, J. F. 1969 *Surface and colloid science*, 1 (eds Matejevic and Eirich). New York: Wiley-Interscience.
Pietsch, W. & Rumpf, H. 1967 *Z. Tech. Chemie*, **15**, 885.
Plateau, J. 1873 *Statiq. expl. et theor. des liquides*, Gand.
Princen, H. M. 1968 *J. Coll. Interface Sci.* **26**, 249.
Princen, H. M. 1969 *Surface and colloid science, 2* (eds. Matejevic and Eirich). New York: Wiley-Interscience.
Radushkevich, L. V. 1952 *Izv. Akad. nauk SSSR Otdel Khim Nauk.* **69**, 1008.

PHILOSOPHICAL TRANSACTIONS OF THE ROYAL SOCIETY A MATHEMATICAL, PHYSICAL & ENGINEERING SCIENCES

Smolders, C. A. 1961 Thesis Utrecht.
Staicopolus, D. N. 1962 *J. Colloid Sci.* **17**, 439.
Staicopolus, D. N. 1963 *J. Colloid Sci.* **18**, 793.
Staicopolus, D. N. 1967 *J. Colloid Sci.* **23**, 453.
Stauffer, C. E. 1965 *J. phys. Chem.* **69**, 1933.
Sugden, S. 1921 *J. Am. chem. Soc.* p. 1483.
Tawde, N. R. & Parvatikar, K. G. 1951 *Indian J. Phys.* **25**, 473.
Tawde, N. R. & Parvatikar, K. G. 1954 *Indian J. Phys.* **28**, 345.
Tawde, N. R. & Parvatikar, K. G. 1958 *Indian J. Phys.* **32**, 174.
Verschaffelt, J. E. 1918 *Verslagen Kon. Akad. v. Wetenschappen Amsterdam*, **27**, 205, 688.
White, D. A. & Tallmadge, J. A. 1965 *J. Fluid Mech.* **23**, 325.

PHILOSOPHICAL TRANSACTIONS OF THE ROYAL SOCIETY A MATHEMATICAL, PHYSICAL & ENGINEERING SCIENCES